ADDIS ABABA UNIVERSITY

COLLEGE OF NATURAL AND COMPUTATIONAL SCIENCE

DEPARTMENT OF CHEMISTRY

A Computational Investigation of Hydrated Magnesium Sulfate Clusters and their FAU Composites for Improved Thermochemical Energy Storage

By

Belaynew Teshome Hailu

Advisor

Dr. Getachew Gizaw

Prof. Ahmed Mustefa

June, 2024

A Computational Investigation of Hydrated Magnesium Sulfate Clusters and their FAU Composites for Improved Thermochemical Energy Storage

Belaynew Teshome Hailu

A Thesis Submitted to The Department of Chemistry

Presented in Partial Fulfillment of the Requirement for the Degree of Master of Science in Chemistry (Physical Chemistry)

Addis Ababa University

Addis Ababa, Ethiopia

June, 2024

ADDIS ABABA UNIVERSITY

COLLEGE OF NATURAL AND COMPUTATIONAL SCIENCE
DEPARTMENT OF CHEMISTRY

This is to certify that the thesis prepared by Belaynew Teshome Hailu, entitled: "A Computational Investigation of Hydrated Magnesium Sulfate Clusters and their FAU Composites for Improved Thermochemical Energy Storage" and submitted in partial fulfillment of the requirements of the Degree of Master of Science in Chemistry (Physical Chemistry) compiles with the regulations of the University and meets the accepted standards with respect to originality and quality.

Signed by the Examining Committee:

Examiner:

1. Dr. Yedilfana Setarge (Internal) Signature _____
2. Dr. Georgies Alene (External) Signature _____

Chairman:

Dr. Girum Ayalneh Signature _____

Advisor:

1. Dr. Getachew Gizaw Signature _____
2. Prof. Ahmed Mustefa Signature _____

_____

Chair of the Department or Graduate Program Coordinator

DECLARATION

I sincerely declare that:

1. I am the sole author of this thesis report.
2. All the information contained in this thesis report is certain and correct to the best of my knowledge,
3. I declare that the thesis report here submitted is original except for the source materials explicitly acknowledged and that this thesis or parts of this thesis have not been previously submitted for the same degree or for a different degree.

Belaynew Teshome Hailu

Student ID: GSR/6330/15

Signature _____

August 11, 2024

Abstract

The effective use of renewable energy sources and the decrease of greenhouse gas emissions are greatly dependent on thermal energy storage, or TES. We report a computational method for examining the hydrate clusters of hydrated magnesium sulfate ($MgSO_4$) and their compounds with faujasite zeolite (FAU) for enhanced performance in thermoelectric sensing (TES). The optimal hydration states and structural characteristics of the hydrated $MgSO_4$ clusters were revealed through modeling with density functional theory (DFT) calculations. Molecular dynamics techniques were used for optimization of composite structure implemented by Vienna Ab initio Simulation Package (VASP) software. After this, the TES capacity, reversibility, and thermal conductivity of the $MgSO_4$ hydrate-FAU composites were assessed. As a result of their superior heat storage properties over their constituent parts, composite materials are a strong contender for advanced thermal energy storage applications, according to the research. This method of computational research gives a logical way to create high-performance thermoelectric solar materials while also shedding light on the interactions at the molecular level.

key words: Composite structure; DFT; FAU-Zeolite; Hydrated magnesium sulfate; MD; Thermal energy storage

In memory to my father, Teshome Hailu

Acknowledgment

I would like to express my sincere feelings of gratitude and appreciation to my advisor, Dr. Getachew Gizaw, for his genuine day-to-day follow-up, advices, guidance, and valuable suggestions, encouragement and continuous dedicated support throughout the period of this work. I also acknowledge my advisor Prof. Ahmed Mustefa for his valuable discussion, support, comment, and scientific suggestions. I would like to express my deepest gratitude to my mother, Haftam Semaw Gashaye, and my wife, Tarik Melakneh, for their persistence, motivation, encouragement, care and love of support throughout my life. I am also indebted to the staff members of Abado Secondary School for their valuable cooperation in all things. I am deeply grateful to everyone who has shown me moral support, encouragement, and remarks at all times.

Contents

List of Figures

List of Tables

Acronyms

AIMD	Ab Initio Molecular dynamics
TCMs	Thermochemical materials
CHARMM	Chemistry at Harvard Macromolecular Mechanics
DFT	Density Functional Theory
ZPE	Zero-point Energy
HB_n	Hydrogen Bonding n=1,2,3,...
P_{H_2O}	Partial pressure of water
PT	Proton Transfer
ESP	Electrostatic potential
GGA	Generalized gradient approximation
XC	Exchange correlation
FAU	Faujasite
IZA	International Zeolite Association
DSC	Differential Scanning Calorimetry
TGA	Thermogravimetric Analysis
VESTA	Visualization for Electronic and Structural Analysis
VASP	Vienna Ab initio Simulation Package
QM	Quantum mechanics

1 Introduction

In this study, improvement of thermochemical energy storage devices store and release energy through reversible chemical reactions is investigated. Because of its high energy density, comparatively low dehydration temperature, and natural abundance, hydrated magnesium sulfate ($MgSO_4 \cdot nH_2O$) has been identified as a possible TCES material. But the structural, energetic, and kinetic characteristics of the material must be thoroughly understood for the design and optimization of thermochemical energy storage (TCES) systems based on hydrated magnesium sulfate, and to make the transition to sustainable energy in the future, innovative materials and technologies with efficient energy conversion and storage must be developed.

A potential solution to the momentary nature of renewable energy sources is TCES devices, which use reversible chemical reactions to store and release thermal energy. Sulfate-bearing hydrated salts are among the different TCES materials that have attracted a lot of interest because of their potential for low-cost manufacture, reversible dehydration chemistry, and relatively high energy densities [1]. The development and refinement of hydrated materials containing sulfate (in our case, $MgSO_4.nH_2O$) for use in TCES applications, however, still presents a substantial difficulty. Attaining better energy density, cycling stability, and heat transfer kinetics necessitates a thorough understanding of the complex interactions between the material's composition, structure, and thermochemical properties. Utilizing computational modeling and simulation methods provides a potent means of methodically investigating the design space and directing the creation of enhanced hydrated TCES materials carrying sulfate.

The advent of composite constructions that integrate hydrated magnesium sulfate and Faujasite (FAU) has led to notable progress in the field of heat storage. These composites improve thermochemical performance by utilizing the special qualities of both components [2]. Strong enough to endure the demands of heat storage applications, the FAU framework is known for its great thermal stability and exceptional ion exchange process capacity. However, the high heat of hydration and phase change characteristics of hydrated magnesium sulfate are important for effective heat storage and release. The composite structure seeks to maximize heat storage capacity and thermal cycle stability by combining both of those components, opening the door for more effective and long-lasting heat storage solutions [3]. The selected hydrated magnesium sulfate for improved thermochemical energy storage

performance is presented in this thesis using a thorough computational method.
This research provides fundamental insights into the structure-property relationships, impregnated hydrated $MgSO_4$ for improvement of kinetics, and thermodynamic behavior of these promising TCES materials by combining advanced computational methods, such as density functional theory and molecular dynamics simulations. The results of this study should aid in the logical design of hydrated magnesium sulfate that is better able to store energy, which will eventually promote the broad use of TCES technologies in the context of renewable energy systems.

1.1 Literature review

Energy produced from unlimited sources (renewable energy) or stored using less-expensive techniques is becoming increasingly important throughout time. Sensible, Latent and thermochemical heat are three different ways that thermal energy can be stored. Solar energy is one of the cleanest renewable energy resources, with the least negative impact on the environment [4]. Solar energy can be captured in physical or chemical forms, depending on the material we use to store it. Sensible heat and latent heat are two ways of storing thermal energy physically, whereas reversible chemical reactions are used for thermochemical heat storage in chemical form. The process of hydrating and dehydrating salt hydrates can be used to store solar energy. The more compact energy storage density is obtained from the thermochemical storage of heat in chemical form [5].
Compact heat storage can benefit from thermochemical form since it has the maximum energy density when compared to other thermal forms. Three important classes of prospective thermochemical materials (TCMs) for seasonal heat storage include salt hydrate, carbonates, and hydroxide [6, 7]. Salt hydrates are in the category of TCMs. These materials break down into a less hydrated or anhydrous condition after absorbing solar energy and charging. These dried salt hydrates release energy when they are mixed again with H_2O [8].
One possible option for thermal energy storage in seasonal heat storage systems is magnesium salt hydrates. Energy exchange throughout the hydration and dehydration processes in $MgSO_4$ is significant (about 2.8 GJ/m^{-3}) [9–11] . Since these salt hydrates are widely distributed in nature, they are superior thermo-chemical heat-storage materials. However, studies have demonstrated that the low degree of hydration under typical air circumstances causes low efficiency in thermo-chemical heat storage systems that use salt hydrates. One of the main areas of attention for the planned thesis research is the degree of hydration and

its major effects on the structural, energetic, and thermal properties of the $MgSO_4$ clusters.

$$MgSO_4 \cdot nH_2O \rightleftharpoons MgSO_4 + nH_2O \quad (1)$$

The reaction moving forward is endothermic, whereas the reaction moving backward is exothermic. Finding materials with a large storage capacity, cycle stability, and quick Kinetics is the main problem in the selection of these salt hydrates [12]. Hepta-hydrated magnesium sulphate dehydrates to lower case and anhydrous form depends on the increase temperature at three stages that start from room temperature.

Experimentally, $MgSO_4.7H_2O$ starts to lose one water molecule between ranges of temperature 273K–328K. The second dehydration stage starts at a temperature of 333K and ranges up to 538K. At this stage, almost all the remaining water molecules are dehydrated and higher amount of energy can be stored in it. Lastly, a fraction of water molecule released when the temperature increased above 540 K. The experimental findings indicate that there are at least three phases involved in the dehydration of $MgSO_4 \cdot 7H_2O$. also indicated in the following reaction [13].

$$MgSO_4 \cdot 7H_2O(s) \rightleftharpoons MgSO_4 \cdot 6H_2O(s) + H_2O(g) \quad \text{at } 25 - 55^{\circ}C \quad (2)$$

$$MgSO_4 \cdot 6H_2O(s) \rightleftharpoons MgSO_4 \cdot 0 \cdot 1H_2O(s) + 5 \cdot 9H_2O(g) \quad \text{at } 60 - 265^{\circ}C \quad (3)$$

$$MgSO_4 \cdot 0 \cdot 1H_2O(s) \rightleftharpoons MgSO_4(\,s) + 0 \cdot 1H_2O(g) \quad \text{at } 275^{\circ}C \quad (4)$$

Because of the need to improve the thermodynamic properties and the sluggish kinetic metastable states included in the hydration processes, the heat storage process in $MgSO_4$ crystals is more complicated [14]. The dehydration energy that is captured by solar radiation during the summer can be retained, and When winter arrives, the system is hydrated to release the stored energy [15]. Nonetheless, the Material properties and the kinetics of the hydration and dehydration reactions are determined as how well these Systems perform. The hydration and dehydration dynamics of these Hydrates are greatly influenced by the crystal structure, surface imperfections, and dislocations that are present. It is known that the kinetics of the $MgSO_4$ hydrates are slow, which may be Caused by the existence of metastable states [16]. In this study, we employ molecular dynamics theory and density functional theory Calculations to investigate the influence of pressure (P_{H_2O}) and temperature on the dehydration process of $MgSO_4 \cdot nH_2O$.

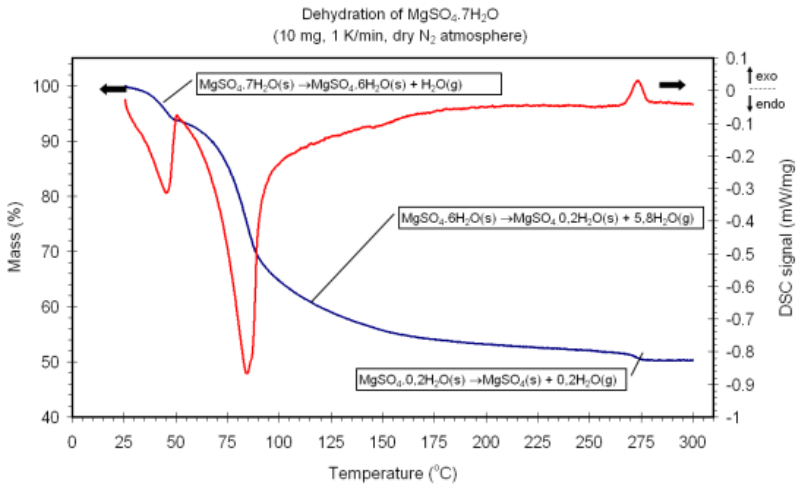

Figure 1: A typical TGA-DSC curve for dehydration of $MgSO_4.7H_2O$.
Image taken from Van Essen etal [13]; The blue line denotes TGA curve, and the red line denotes the DSC curve

1.1.1 The Time-Independent Schrödinger Equation

The independent of time a key equation in quantum chemistry, the Schrödinger equation defines how a particle behaves in a potential that employee to ascertain a system's wave function and energy levels. The time-independent Schrödinger equation is given by:

$$\hat{H}\psi(\vec{r}) = E\psi(\vec{r}) \tag{5}$$

where: $\hat{H}$ is the Hamiltonian operator, which represents the total energy of the system. $\psi(\vec{r})$ is the wave function, which describes the state of the particle as a function of the spatial coordinates $\vec{r}$. E is the energy eigenvalue, which represents the allowed energy levels of the system. The Hamiltonian operator, $\hat{H}$, can be written as:

$$\hat{H} = -\frac{\hbar^2}{2m}\nabla^2 + V(\vec{r}) \tag{6}$$

where: $\hbar$ is the reduced Planck constant. m is the mass of the particle. ∇^2 is the Laplacian operator, which represents the kinetic energy term. $V(\vec{r})$ is the potential energy function, which represents the potential energy of the particle in the system. Substituting the Hamiltonian operator into the time-independent Schrödinger equation, we get:

$$-\frac{\hbar^2}{2m}\nabla^2\psi(\vec{r}) + V(\vec{r})\psi(\vec{r}) = E\psi(\vec{r}) \tag{7}$$

1.1.2 Techniques for Solving the Schrödinger Equation

Various computational techniques have been developed to solve the Schrödinger equation, including: The basic equation of quantum mechanics which is time independent Schrodinger equation, can be expressed as follows:

A. **Density Functional Theory (DFT)**

Density functional theory is a computational technique that involves rewriting the Schrodinger equation in terms of electron density as opposed to the many-body wavefunction. To mimic the interactions between electrons, a variety of exchange-correlation functionals have been created inside the DFT framework, making DFT applicable to a broad range of solid-state and molecular systems. DFT is a computational method that provides valuable insights in the atomic and electronic structure, as well as the Energetics of materials [17].

The whole many-body wave function is not represented by DFT, which greatly decreases computational complexity. Instead, it depicts the electron density and which is Methods for solving the Schrodinger problem numerically which have been devised. The foundation of DFT lies in the Hohenberg-Kohn theorems, which establish a one-to-one relationship between the external potential and the ground-state electron density [18].

As a result, the many-body problem can be effectively reduced to a single-particle problem that can be resolved more quickly. In quantum chemistry and materials science, DFT has become a popular computational technique because it can yield accurate results for a variety of systems, such as solids, molecules, and surfaces, at a relatively low computational cost when compared to more accurate but computationally intensive ab initio methods. DFT is an effective method for researching and creating novel materials with desired features since it has proven successful in predicting the electronic structure, energetics, and other properties of materials [18, 19].

B. **Molecular Dynamics (MD)**

MD simulations solve the time-dependent Schrödinger equation by propagating the wave function in small time steps, allowing for the study of the dynamics of atomic and molecular systems. By solving Newton's equations of motion, molecular dynamics is a computational technique that mimics the motion of atoms and molecules [18]. Although MD does not directly solve the Schrodinger equation, it can be coupled with quantum mechanical techniques to examine the time evolution of quantum systems. This method splits the system into two sections: a classical portion that treats the atoms according to classical mechanics,

and a quantum mechanical region that solves the Schrodinger equation.
A quantum mechanics/molecular mechanics (QM/MM) framework is used to characterize the interactions between the two domains. Large-scale systems, like proteins or materials, where the quantum effects are restricted to particular regions of interest, can be studied thanks to this hybrid technique. The dynamical behavior of quantum systems, including the impact of thermal fluctuations and the function of nuclear mobility in chemical reactions and material characteristics, can be better understood by MD simulations [18, 19].

1.1.3 Composite Structures

Because thermal energy improvement in dehydration and slow kinetics in dehydration are disadvantages, scientists are investigating composite structures that can accelerate the rate of dehydration while preserving the advantageous characteristics of hydrated magnesium sulfate [10].
Zeolites are porous metal oxides having pore dimensions in the range of 3–13 Å. Zeolites have high kinetic properties but a low energy density, and due to this, they are selected for making composite structures. They are usually aluminosilicates and have large cavities and distinct channel geometries.For about 250 years, people have been aware of zeolites, which are crystalline minerals that are widely found in the natural world. When a naturally occurring mineral called stilbite was heated, a lot of its steam was released, as found by Axel Fredrick Crønstedt in 1756. So he called the substance ”zeolite,” a term that comes from classical Greek, where zeo means ”to boil” and lithos means ”stone” [20].
According to the International Zeolite Association’s (IZA) database, there are different types of zeolites depending on their building scheme, and one of them is the Faujasite (FAU) zeolite. The adsorption and porosity of FAU-zeolite make it a perfect substitute for addressing the sluggish rate of dehydration of hydrated magnesium sulfate. The FAU-zeolite’s linked cavities and channels offer a clear framework structure that is able to hold the hydrated magnesium sulfate molecules. FAU-zeolite and hydrated magnesium sulfate can be combined to form a composite structure that improves the dehydration process by utilizing the special qualities of both components [21].

1.1.4 Structural Aspects of FAU-Zeolites

An infinitely extending three-dimensional network of $[SiO_4]^{4-}$ and $[AlO_4]^{5-}$ tetrahedra connected to one another by the sharing of oxygen atoms forms the basis of zeolites, which are crystalline, microporous, hydrated aluminosilicates [22]. There are various benefits to incorporating FAU zeolite into the composite structure.

First of all, FAU-zeolite's porous structure increases the surface area available for interacting with water molecules, which promotes their adsorption and eventual dehydration [23]. By functioning as a potent adsorbent and boosting the stability and reactivity of the composite system, the FAU zeolite contributes significantly to the improvement of the thermochemical performance of hydrated magnesium sulfate. Recent research indicates that adding FAU zeolite to hydrated magnesium sulfate composites may greatly boost the material's adsorption capacity as well as its heat storage density and efficiency [24].

Furthermore, the FAU zeolite's wide surface area and distinct pore structure may make it easier for reactants and moisture to move across the hydrated magnesium sulfate phase, encouraging the dehydration process and improving the system's overall thermochemical performance. Consequently, there is a lot of promise for developing and refining new materials for energy storage applications through the use of FAU zeolite.

The FAU zeolite's exact structural properties, such as the opening width of its 12-membered ring windows (about 7.4 Å), are critical in determining its applicability for a variety of activities, including adsorption, catalysis, and energy studies [25].

The FAU zeolite's performance may be optimized in various applications due to its capacity to adjust the Si/Al ratio and, in turn, the pore size and acidity. and its structure is shown below [25, 26]. Therefore, primitive FAU zeolite ($Si_{48}O_{96}$), which exactly represents conventional zeolite and can simplify computational cost, is selected for our specific purpose of studying the adsorption, disorption, and thermal properties of composite materials in super cages and some sodalite cages for lower hydrate.

1.1.5 Lowenstein's rule and Position of cations

Lowenstein's rule, which asserts that Al-O-Al connections are categorically prohibited in aluminosilicate frameworks, is a fundamental tenet guiding the FAU structure [27]. This indicates that at least one silicon (Si) atom must exist between each aluminum (Al) atom in order for them to be physically bonded to one another.

In the FAU framework, where the intervening Si atoms isolate the Al atoms from one

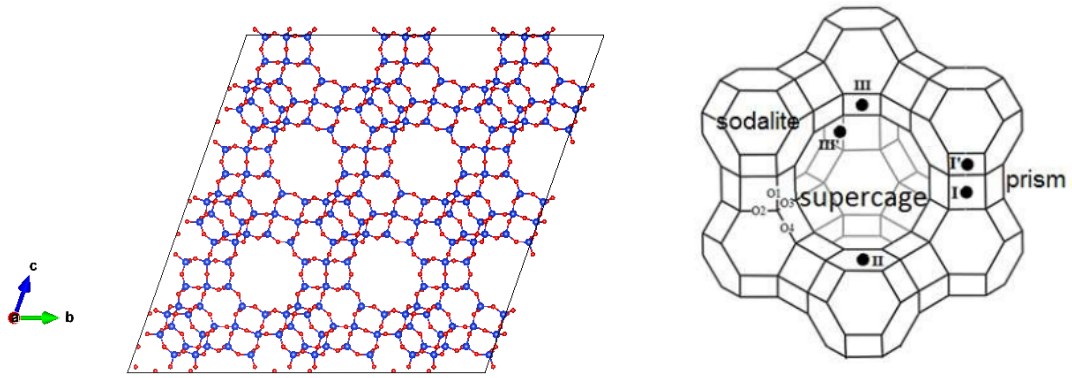

Figure 2: Primitive Faujasite unit cell and crystallographic positions in the supercage, sodalite and prism cages.

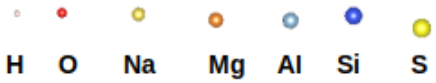

Key: different colors of spheres are used to represent atoms throughout this thesis.

another, this criterion is carefully adhered to. The general chemical formula for the FAU structure can be written as $M_{x/n}[(AlO_2)_x(SiO_2)_{y-x}] \cdot wH_2O$, where M represents the charge-balancing cations, n is the charge of the cation, x is the number of Al atoms per unit cell, y is the total number of T-atoms (T = Si, Al) per unit cell, and w is the number of water molecules per unit cell [28]. The following nomenclature is frequently used to refer to the charge-balancing cations in the FAU structure: sodium (Na^+) as Na-FAU, potassium (K^+) as K-FAU, calcium (Ca^{2+}) as Ca-FAU, and magnesium (Mg^{2+}) as Mg-FAU [2]. The adsorption, catalytic, and ion-exchange capacities of the zeolite material, as well as its physicochemical properties, can be strongly influenced by the arrangement and distribution of these cations inside the FAU framework [29].

One of the main reasons FAU zeolites are used so widely is because of their tight adherence to Lowenstein's rule, which results in a well-defined and stable aluminosilicate framework. This covers their application as ion-exchangers, adsorbents, and catalysts in a range of industrial processes. A number of variables, such as the kind of cation, the circumstances surrounding zeolite production, and the existence of guest molecules, might affect the distribution and placement of cations inside the FAU structure. The properties of the FAU zeolite are greatly influenced by the dynamic nature of the cation dispersion, which opens up a variety of uses in ion exchange, adsorption, and catalysis. [28, 29].

1.2 Problem of Statements

Technologies for TES are essential for reducing greenhouse gas emissions and making effective use of renewable energy sources. Unfortunately, the low thermal conductivity, poor reversibility, and limited energy storage capacity of several existing TES materials prevent them from being widely used. Due to their high energy storage density and phase shift characteristics, hydrated salts such as magnesium sulfate hydrates have demonstrated promise as TES materials. Furthermore, by improving heat transfer and structural stability, the addition of zeolites like faujasite may improve these materials' thermal characteristics. The development of a computational investigation technique is necessary to understand the underlying mechanisms and optimize the performance of hydrated MgSO4 clusters and their composites with FAU zeolite for enhanced TES applications.

These issues must be addressed. This thesis specifically addresses the following problem: What are the underlying structural and thermodynamic factors governing the performance of hydrated $MgSO_4$ clusters and their FAU composite materials, and how can their computational design improve thermal energy storage capacity, reversibility, and thermal conductivity compared to the individual components?

The proposed research seeks to solve this problem statement in order to offer a logical design framework for the creation of advanced TES materials with improved performance, which can aid in the larger objective of sustainable energy storage and consumption.

1.3 Objectives

1.3.1 General Objective

The general objective of the thesis titled "A Computational Investigation of Hydrated Magnesium Sulfate Clusters and Their Composites for Improved Thermochemical Energy Storage" is to conduct a computational investigation of hydrated magnesium sulfate clusters and their composites to enhance the understanding of their potential for improved thermochemical energy storage (TCES) performance.

1.3.2 Specific objectives

The goal of this research is to create and evaluate a composite substance based on magnesium sulfate for enhanced thermochemical performance and improved thermal energy storage.

1. Creating and optimizing clusters of hydrated magnesium sulfate using the CHARMM force field and VASP software.

2. Analyze the stability, charge distribution, and energetics of the hydrated magnesium sulfate clusters to identify key factors that affect their thermochemical behavior.

3. Investigate the thermodynamic properties of the dehydration reaction of the hydrated magnesium sulfate clusters under varying pressure and temperature conditions.

4. The purpose of this study was to develop composite structures of optimized structures using FAU and to validate the computational design framework by demonstrating the improved thermochemical performance of the optimized sulfate-bearing materials.

2 Computational Details

2.1 Molecular Mechanics

Artificial bee colony algorithm was used to generate any possible structure for the successful input cluster preparation of $MgSO_4$. For the global optimization of chemical cluster structures, this type of algorithms uses CHARMM, which is the most effective, potent, and well-liked programs. The tasks for Conformation search for molecules become routine due to the fundamental artificial bee colony algorithm [30]. We generate 30 possible structures for anhydrous and hydrated form of magnesium sulphate for each case and among them, one structure with global minimum and the remaining 29 structures are other possible structures with local minimum. Among the 30 possible structures generated, with global minimum and a local minimum with lower energy are selected for further optimization using DFT. All selected structures are optimized by DFT using The Vienna Ab initio Simulation Package (VASP) software.

VASP is a widely used and highly regarded software package for performing ab initio quantum-mechanical, molecular dynamics (MD) and simulations based on density functional theory (DFT).The software utilizes plane-wave basis set and pseudo-potentials to represent the wave functions and electron-ion interactions in the system. It is also computer program for atomic-scale materials modelling, e.g. electronic structure calculations and quantum-mechanical molecular dynamics, from first principles [31]. In the context of density functional theory (DFT) or the Hartree-Fock (HF) approximation, VASP calculates an approximate solution to the many-body Schrödinger equation by solving the Kohn-Sham equations [32].

After we optimized by the help of VASP, only one structure was selected for further studies of thermal properties, like total energy, which is the sum of electronic energy gained from optimization, zero-point energy (ZPE) and thermal correction. Here, Gibbs free energy is important because it is dependent on the two variables of pressure and temperature. Therefore, we carefully selected one structure with minimum energy for further computation the vibrational aspect for ZPE and thermal correction because it is very expensive, type of calculation. The frequencies that are utilized for the computation of zero-point energies and other thermal adjustments to the overall energy are likewise scaled. For example, the frequency should be free from imaginary, and there are differences in the best scaling factors

for these various applications [16, 33]. During optimization, some structures of hydrated magnesium sulphate like mono-, di-, and hexa and hepta-hydrated magnesium sulphate take part in a proton transfer, which may happened because of acidity/basicity of groups in the structure and is not important for our study, which is further discussed in section 3. Due to proton transfers, these structures, we considered the second structures with lower energy intact water for further studies of thermal property.

2.2 Method Validation

VASP (Vienna Ab initio Simulation Package)is a widely used software package based on DFT for simulating and modeling materials at the atomic scale.It employs the projector-augmented wave (PAW) method or ultrasoft pseudopotentials to describe the interaction between the valence electrons and the ionic cores. This approach reduces the computational cost by representing the core electrons with effective potentials while accurately describing the valence electrons.

The accuracy and reliability of computational results obtained from VASP are most importance. Method validation is a critical step to ensure that the software produces consistent and accurate results [32]. Molecular structures of various hydrates (0, 1, 2,... 7) of $MgSO_4$ were optimized using the density functional level theory using plane wave polarization of generalized gradient approximation (GGA) XC functional, optPBE-vdW-DF2 which includes different energy like exchange energy, self-interaction energy, and correlation energy and kinetic energy [31].

The energy difference to carry out self-consistent field is 10^{-5}eV for the first structural refinements,10^{-6}eV for further optimization and 10^{-8}eV for frequency calculations. 11 angostroms were used in three directions to minimize interactions for vacuum setup with the force exerting less than 0.01 eV per atom. In this case, VASP is a highly versatile and powerful tool for computational materials science and is widely used in academia and industry. Its accuracy, reliability, and continuous development by a dedicated team of researchers and developers have made it a standard software package in the field of computational materials science and solid-state physics [34].

2.3 Methodology

2.3.1 statistical Mechanics Approach

We optimize the structures of several hydrates of $MgSO_4 \cdot nH_2O$, where n = 0.1 – 7. The systems in this study relate to molecules in the gas phase because solution effects are not taken into consideration. In this work, structural optimization is carried out for each individual hydrated and anhydrous structure that is covered. Additionally, a frequency analysis is performed to verify that imaginary frequencies are absent. At a higher level (n = 6 and 7), we selected two possible structural isomers for each n value to mimic the bulk structures which depend on the coordination of oxygen atoms on magnesium. The two possibilities are when a metal coordinates with one oxygen-sulphur atom, and the other is when a metal binds with two oxygen-sulfur atoms.

To compute ΔG of the dehydration and hydrolysis reaction, information on vibrational spectra, ground state geometry, and Gibbs free energy (G) of all reactants and products are required. The dehydration of magnesium sulfate takes place in a temperature of range that may be covered by medium temperature collectors (around 150°C), the second dehydration stage has a high energy density of $2.2 \pm 0.1\ GJ/m^3$, and melting of the $MgSO_4 \cdot 7H_2O$ can be prevented.

$$MgSO_4.7H_2O \rightleftharpoons MgSO_4 \cdot nH_2O + (7 - n)H_2O \quad for\ n = 6, 4, 1, and\ 0 \tag{8}$$

Because of this, compact seasonal solar heat storage finds this phase to be the most interesting . The following dehydration reactions of $MgSO_4$ hydrate are relevant to us in our study and because of the need for calculating thermodynamic parameters [13]:

$$MgSO_4 \cdot 6H_2O \rightleftharpoons MgSO_4 \cdot nH_2O + (6 - n)H_2O \text{ for } n = 2, 1, 0 \tag{9}$$

$$MgSO_4 \cdot 2H_2O \rightleftharpoons MgSO_4 \cdot nH_2O + (2 - n)H_2O \ for\ n = 1, 0 \tag{10}$$

$$(MgSO_4)_2.12H_2O \rightleftharpoons (MgSO_4)_2.nH_2O + (12 - n)H_2O \ for\ n = 5, 3, 1 and 0 \tag{11}$$

For the reactions mentioned above, the change in Gibbs free energy is expressed as

$$\Delta G = \sum G_{\text{products}} - \sum G_{\text{reactants}} \tag{12}$$

$$\Delta_{\text{deh}} G = \Delta_{\text{rxn}} G + RT \ln Q \tag{13}$$

Where $\Delta_{\text{deh}} G$, $\Delta_{\text{rxn}} G, R, T$ and Q represent the change in the Gibbs free energy of dehydration, the change in the Gibbs free energy of reaction, the constant molar gas and the temperature of the system, respectively. Putting $\Delta_{deh}G$ to zero, the equilibrium product concentration of the dehydration reactions can be found. The physical condition of every reactant and product matters for the ΔG computation. In the experimental setup, H_2O exists in the gaseous phase, whereas $MgSO_4$ hydrates stay in the solid phase. However, accurate determination of frequency, and hence the Gibbs free energy of solid $MgSO_4$ hydrates over a broad temperature range, presents a computational challenge [16].

$$\log\left(\frac{p_{H_2O}}{p^o}\right) = \frac{-\Delta_{r\times n}G}{2.303nRT} \tag{14}$$

Where p^o is standard atmospheric pressure, which is 1 atm and n is the coefficient of water when the dehydration equation is balanced. The calculation of the Gibbs free energy of the crystalline phase is costly because of the huge sizes of the Mg, S, and O atoms, as well as the large number of atoms in each unit cell. In a solid-gas reaction, the gaseous phase's Gibbs free energy (G_{gas}) can be used to determine the ΔG. In seasonal heat storage systems, the equilibrium product concentration determined under the gas assumption will be regarded as the reaction's safety limit. The dehydration reaction's ΔG is calculated in this work using the ideal polyatomic gas assumption, which assumes that both the reactant and the product are in the gaseous condition [35]. For a given temperature T and absolute pressure p, the Gibbs free energy of the gaseous molecule is [36]:

$$G(T, P) = U + PV - T\Delta S \tag{15}$$

An ideal polyatomic gas's partition function is given as:

$$q = q_{\text{trans}}\, q_{\text{rot}}\, q_{\text{vib}}\, q_{\text{elec}} \tag{16}$$

Where q is the partition function and $q_{trans}, q_{rot}, q_{vib}$, and q_{elec} are their translational, rotational, and electronic contributions. Internal energy (U) of poly-atomic gas can be expressed as [36]

$$\mathrm{U(T,P)} = 3\mathrm{RT} + \mathrm{R}\sum_{j=1}^{3N-6}\left(\frac{\Theta vib\,j}{2} + \frac{\Theta vib\,j}{e^{-\Theta vib\,j/T}-1}\right) + U_{gr} \tag{17}$$

Where R is the gas constant, $\Theta vib\,j$ is vibrational temperature, $(\mathrm{h}\nu/\mathrm{k_b})$ of the $\mathrm{j^{th}}$ atom, ν is the frequency of the vibrational mode, h is Planck's constant, $\mathrm{k_b}$ is the Boltzmann constant, and $\mathrm{U_{gr}}$ is the ground state energy of the molecule. The polyatomic gas entropy (S) can be written as follows:

$$S(T,P) = R\left[\left(\frac{K_bT}{p}\left(\frac{2\pi MK_bT}{h^2}\right)^{3/2}\right)+\frac{3}{2}\right] + R\sum_{j=1}^{3N-6}\left(\frac{\Theta vib,\, j/T}{e^{\mathrm{evibjT}}-1}\right) + R\sum_{j=1}^{3N-6}\left[\ln\left(1-e^{-\theta vibjTT}\right)\right] + S_{\mathrm{rot}} \tag{18}$$

Where $\mathrm{S_{rot}}$ is the rotational contribution of entropy and M is the total atomic mass. This expression can be used to represent the asymmetric top molecule, as indicated below [36].

$$S_{\mathrm{rot}} = R\left[\ln\left(\frac{\sqrt{\pi I_aI_bI_c}}{\sigma}\left(\frac{8\pi^2k_bT}{h^2}\right)^{3/2}\right)+\frac{3}{2}\right] \tag{19}$$

Where the three principal moments of inertia are represented by $\mathrm{I_a}, \mathrm{I_b}$, and $\mathrm{I_c}$, while the number of rotational modes in the molecule is denoted by its symmetry number, σ. Equation (20) is used to compute the zero-point energy, $\mathrm{U_{ZPE.}}$.

$$U_{ZPE} = R\sum_{i=1}^{3n-6}\frac{hvi}{2k_bT} \tag{20}$$

The solvation characteristics of molecules and ions can be predicted with the use of knowledge about the dehydration energy. When estimating the viability and spontaneity of chemical processes involving the addition or removal of water molecules, including dehydration and hydration reactions, it is essential to consider the dehydration energy per mole of water. An energy-unfavorable water removal process is indicated by a high dehydration energy per mole of water, whereas a low dehydration energy implies a more favorable dehydration process.

$$\Delta E_{dehd} = \frac{1}{m}(E_{MgSO4.n-mH2O} + mE_{H2O} - E_{MgSO4.nH2O}) \tag{21}$$

We have determined the ground state energy and frequency of the molecule's vibrational mode based on the optimized geometry. Equations (12) and (13) are used to determine the ΔG of a specific dehydration reaction on a given T and P.

2.4 Methods of Making Composite structures

Molecular dynamic simulations, or first principle calculations, are used in theoretical methods for adsorption in porous materials, and PACKMOL is used for making composite structures with the parameters being studied. Four exchange-correlation functional were compared within this work: the PBE functional, PBE-D3, optPBE-vdw, and rev-optPBE-vdW-DF2 are computed using ISIF 2, for 3 and 8 geometry relaxation, and only PBE-D3 ISIF-2 is selected because we want to relax the degrees of freedom of only position, but cell shape and cell volume are fixed. To cut down on computing work, a primitive rhombohedral cell—one-fourth of a conventional cell—was employed in this investigation. Following relaxation at the PBE + D3 level of theory, the lattice parameters of the primitive cell were a = b = c = 17Å and $\alpha = \beta = \gamma = 60^o$, with a unit cell volume of = 3800 $Å^3$. The

```
ALGO = Fast
EDIFF = 10-5
EDIFFG= -0.03
ENCUT = 400  # check
IBRION = 2
ISIF = 2
#ISPIN = 2
LCHARG = False
LREAL = Auto
LWAVE = False
NSW = 1000
PREC = Accurate
ISMEAR=0
SIGMA = 0.1
GGA      = PE
IVDW=11
```

Figure 3: INCAR parameters for optimizing Composites

Perdew Burke Ernzerhof (PBE) exchange-correlation functional in the generalized gradient approximation (GGA) was used in the DFT calculations, which were carried out using VASP. Electron-ion interactions were described using the projector augmented plane wave (PAW) method, and the Kohn–Sham equations were solved self-consistently until the global break condition for the electronic self-consistent loop cycles was less than 10^{-5} eV, and EDIFFG for ionic relaxation was stopped at 10^{-3} eV. The plane wave cut-off energy was set

at 400 eV.

To improve total energy convergence, the broadening in electron volt (eV) was applied to the tetrahedron method, and the Blöchl correction with $\sigma = 0.1$ eV was applied to the band occupations. The atomic positions were fully optimized until the force differences between two successive ionic steps were no more than -0.03 eV per atom. In composite materials, adsorption energy can play a significant role in determining the properties and performance of the material. It affects various aspects, such as the stability of adsorbed species, the efficiency of chemical reactions that occur on the surface, and the overall surface reactivity. For a given optimized and stable structures of hydrated and anhydrous magnesium sulfate in a zeolite, the adsorption energy of the composite structure was calculated as follows [26,37]:

$$E_{ads(\mathrm{MgSO_4}/FAU)} = E_{\mathrm{MgSO_4}/FAU} - E_{\mathrm{MgSO_4}} - E_{FAUpristine} \tag{22}$$

$$E_{ads(\mathrm{MgSO_4 \cdot nH_2O}/FAU)} = E_{\mathrm{MgSO_4 \cdot nH_2O}/FAU} - E_{\mathrm{MgSO_4 \cdot nH_2O}} - E_{FAUpristine} \tag{23}$$

The electronic energy in this case is represented by the first term on the right, which is the structure optimization of anhydrous/hydrated magnesium sulfate adsorbed in the FAU-zeolite's pores (adsorption complex); the second term is the energy of the optimized, isolated magnesium sulfate anhydrous/hydrated; and the third term is the energy of the guest or free pristine zeolite framework. The following equation was used to calculate the interaction energy between the molecule of hydrated/anhydrous magnesium sulfate and the FAU zeolite formulations at 0 K in order to explain the adsorption events [38].

$$\Delta E_{int} = E_{FAU} + E_{molecule} - E_{FAU-molecule} \tag{24}$$

Subsequently, employing the PBE-D3 DFT approach, the primitive Y-type FAU zeolite structure—which constitutes one-fourth of the conventional FAU zeolite and precisely reflects it with a Si/Al ratio of 2.69 was prepared according to Lowenstein's rule [39] and was relaxed using the ISIF 2 (fixed ionic locations and cell shape) relaxation strategy. For an accurate description of intermolecular interactions in zeolite systems, dispersion forces are taken into account using the PBE-D3 functional. Sodium (Na) ions are introduced to preserve the charge equilibrium within the zeolite structure, according to established sites [40,41].

Sodium ions are frequently employed as charge-balancing cations in zeolites because of their compatibility with the FAU structure and relatively low charge density. One way that the negative charge caused by the addition of aluminum (Al) to the zeolite structure is counteracted is by the presence of sodium ions [27, 28]. Thermodynamic computations, including those involving Gibbs free energy, can shed light on the phase behavior and stability of the composite structure. These calculations can give information on phase transitions or the release of water molecules during dehydration, as well as the circumstances in which the composite is thermodynamically advantageous [42].

Here, we use a systematic approach for the calculation of the frequency in all structural optimizations, keeping the location of the structure atoms fixed except for the atom bound to hydrated / anhydrous magnesium sulfate. It is called bad, but there is no option due to the large number of atoms for the calculation of the DFT. However, it is obvious that a comprehensive DFT approach should account for the local relaxations of the zeolite framework following guest molecule adsorption. When examining the mechanical characteristics and structural integrity of composite materials composed of FAU (faujasite) and $MgSO_4 \cdot nH_2O$ the computation of deformation energy is essential.

The potential uses of these kinds of composite structures in ion exchange, adsorption, and catalysis make them interesting. The amount of energy needed to cause a particular structural alteration or deformation in the composite material is represented by the deformation energy. Through precise computation of the deformation energy, scientists can acquire important knowledge on the material's ability to withstand stress, strain, and possible failure mechanisms [43]. In order to ensure that the composite structure can resist anticipated operating conditions and external loads without affecting its integrity or performance, this knowledge is crucial for its design and optimization.

The term "deformation energy" describes the amount of energy needed to change the isolated equilibrium structures of the separate components, in this case, the $MgSO_4$ clusters and the FAU zeolite framework, into the final composite arrangement. The ability of the components to adjust and change structurally is quantified by this deformation energy, which has a major effect on the composite material's overall stability and reversibility. The structural alterations and strain that are induced inside the composite structure during the creation or cycling processes can be better understood by analyzing the deformation energy. In order to calculate the deformation energies, single-point calculations utilizing plane wave

basis sets were also performed for portions of the optimized structures [44]:

$$\Delta E_{deform,FAU} = E_{FAU,config} - E_{FAU-pristine} \tag{25}$$

$$\Delta E_{deform,molecule} = E_{molecule,config} - E_{molecule} \tag{26}$$

Where $\Delta E_{deform,molecule}$ is the change in deformation energy of FAU during impregnation, $E_{FAU,config}$ and $E_{molecule,config}$ are the energy of FAU and molecules after a guest molecule is impregnated, obtained from single point calculation. The knowledge of the stability and performance of the system is largely dependent on the deformation energy, interaction energy, and adsorption energy of the composite structure consisting of hydrated magnesium sulfate ($MgSO_4$) clusters and faujasite (FAU) zeolite, as assessed through computational analysis.

3 Results And Discussion

3.1 Molecular Structures of Magnesium Sulfate ($MgSO_4$), Magnesium Sulfate hydrates and their conformers

Magnesium sulphate ($MgSO_4$) can exist in different hydrate forms, each with a different number of water molecules per formula unit. The conformers of these hydrates depend on the arrangement of the water molecules around the magnesium sulfate complex [45]. The specific conformations can vary, and the water molecules may exhibit different orientations and interactions with the magnesium sulfate ions. However, the overall molecular structure of the hydrates remains the same, with the water molecules coordinated around the magnesium ion and interacting with the sulphate ion. One of the previous studies on the structure of hydrated magnesium sulfate using the computational molecular mechanics method shows us the formation of a long-chain linear structure, which was wrong and completely different from our findings due to the formation of hydrogen bonds [46].

Hydrogen bonds are essential to the integrity of the hydrate structure and its preservation of its ordered arrangement in the case of hydrated magnesium sulphate. In order to provide a stable coordination environment, the hydrogen bonds aid in the arrangement of the water molecules around the magnesium and sulphate ions. It's important to note that the molecular structures of hydrates are subject to changes in different conditions, such as temperature and pressure. These conditions can affect the arrangement and stability of the water molecules within the hydrates. The optimum structures of $MgSO_4.nH_2O$ molecules have been examined in the sections as follows:

3.1.1 Anhydrous and Mono hydrated Magnesium Sulfate

The anhydrous form of magnesium sulfate does not contain water molecules. Its molecular structure consists of one magnesium ion (Mg^{2+}) bonded to one sulphate ion (SO_4^{2-}) with bond length of each two Mg-O are 1.864 Å with relatively good agreement from experimental results, which is 2.094 Å [47]. Two oxygen atoms of the SO_4^{2-} tetrahedral form a bond to the Mg atom in the structure $MgSO_4$ (Figure 5). This structure was obtained from VASP optimization, where we had two possible structures, i.e. one oxygen of sulphate group bonded to magnesium atom and the second one is two oxygen atoms of sulphate group bonded to magnesium atom. But both of them are convergent in the same way, and the result is shown

in Figure 4 after optimization. The Quantum Theory of Atoms in Molecules (QTAIM), sometimes referred to as the Bader charge analysis or Bader analysis, is a technique for dividing a molecule's electron density into atomic components. The distribution of electrons within a molecule can be inferred from the resulting Bader charges, which can have various implications for comprehending the molecule's structure and characteristics [14].

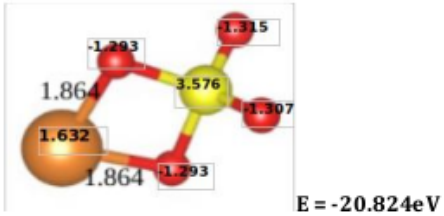

Figure 4: Bader charge and structure of $MgSO_4$ and their Mg-O bond length (Å)

Hydrates of magnesium sulphate, commonly known as Epsom salt, has a chemical formula of $MgSO_4 \cdot nH_2O$, where "n" represents the number of water molecules associated with each magnesium sulphate unit and can form hydrogen bonds between the water molecules and the sulphate ions or between water molecules themselves. In the instance of $MgSO_4 \cdot H_2O$ (Figure 5), introducing a water molecule does not significantly alter the bond lengths in comparison to the other hydrate from anhydrous one but the Mg-O bond length of the new added water molecule is higher than the other Mg-O bond length which is 2.014 Å and there is no hydrogen bond (HBn) formed. Here, we considered the second possible structure as a result of proton transfer in the first most stable structure, which will be discussed in a separate section. The electronic energy difference between the two structures is about -0.989 eV.

A measurable indicator of the electron density on each atom in a molecule is provided by Bader charges. They provide information about how charge are distributed, including how electrons are transferred between atoms and whether charged species—such as cations or anions—are present in the molecule. Understanding the molecule's stability, bonding, and reactivity can be aided by this knowledge.

The type of chemical bonds that exist within a molecule can be examined using Bader charges. The amount of electron transfer or electron density sharing, between linked atoms can be measured by comparing their Bader charges. This gives a quantitative indication of bond polarity and helps define the type of bonding, such as covalent, ionic, or polar covalent. A molecule's electrostatic potential (ESP) can be computed using Bader charges. The ESP

is a useful property to have when studying molecular interactions such as hydrogen bonding or molecular recognition. It sheds light on the electrostatic forces regulating molecular interactions and aids in the comprehension of the spatial distribution of electronic charge. Bader charges can be used to examine a molecule's reactivity and role in chemical processes. Predicting reaction locations and evaluating electron flow during chemical transformations can be made easier with an understanding of charge distribution. Bader charges in catalysis can be utilized to investigate the processes of charge transfer at active sites and direct the development of more effective catalysts. The electronic energy of higher anhydrous

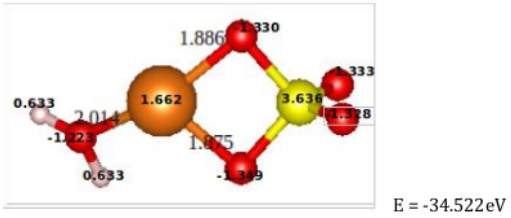

Figure 5: Bader charge and structure of mono hydrated $MgSO_4$ with their Mg-O bond length (Å)

molecules increases as the coordination number and number of atoms increase, as shown in figure 6.There are also different isomers that are identified with a given value of n cluster, depending on their electronic energy; we only focus on the most stable structure, isomer I, and hydrated cases.

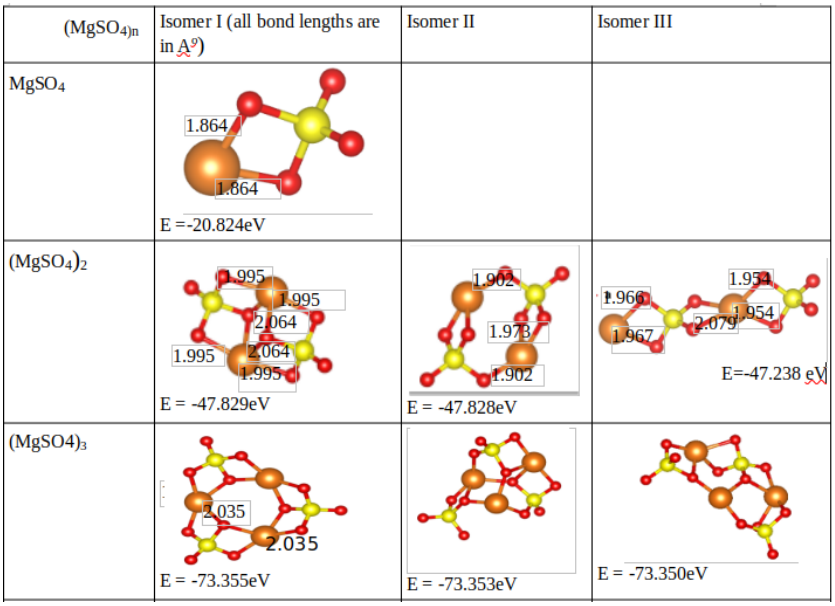

Figure 6: Some Higher clusters of Magnesium sulfate and their corresponding Mg - O bond length

3.1.2 $MgSO_4.2H_2O$ and $MgSO_4.3H_2O$

The presence of hydrogen bonds with different bond lengths characterizes the structures of higher hydrates and hydrogen bonds plays a crucial role in stabilizing the structure of the hydrate. Visualization for electronic and structural analysis (VESTA) visualization software allows us to identify the existence of hydrogen bonds for the given structure. Hydrogen bonds are classified by G. A. Jeffrey as ”strong, mostly covalent” at donor acceptor distances between 2.2 and 2.5 Å, ”moderate, mostly electrostatic” between 2.5 and 3.2 Å, and ”weak, electrostatic” between 3.2 and 4.0 Å. In figure 7a, hydrogen binds with the next oxygen atom of $MgSO_4{\cdot}2H_2O$ making hydrogen bond with a length of O–H 1.998Å, and the O–O bond length is 2.931Å, which is under moderate strength, mostly electrostatic, according to G. A. Jeffrey. The SO_4^{2-} tetrahedral does not undergo significant structural deformation because of these hydrogen interactions.

In the case of tri hydrated magnesium sulfate, one hydrogen bond was visualized (Figure 7b), namely HB1 with an O-H length of 1.517 Å. This hydrogen bond may be considered as strong, and due to that, the O-O distance in HB1 is 2.554 Å. Furthermore, the water molecules linked to these connections have lesser elongations in their O-H bond lengths because of these hydrogen bonds. The general movement of the O atoms connecting the Mg and S atoms toward the S atom is another obvious deformation in the $MgSO_4{\cdot}3H_2O$ structure. This could be because when the degree of hydration rises, the positive charges in the magnesium and sulphur atoms increase. A paper reported by Eldhose Iype et.al shows that there are two hydrogen bonds in dihydrate and three hydrogen bonds in trihydrate magnesium sulfate, which are found using Jeffrey approximation method and disagreed with our work that we are carrying out [14].

Out by the support of VESTA visualization, which is important to easily visualize all the created hydrogen bonds, as shown in all figures named as HBn. In similar manner, we consider the second structure for di hydrated magnesium sulphate due to proton transfer in the first isomer. The electronic energy difference between the structures that experience proton transfer and the next stable structure, which is in figure 8a is also about -0.223 eV. Figures 8a and 8b below are different possible isomers of di hydrated and tri-hydrated magnesium sulphate with their corresponding electronic energy respectively.

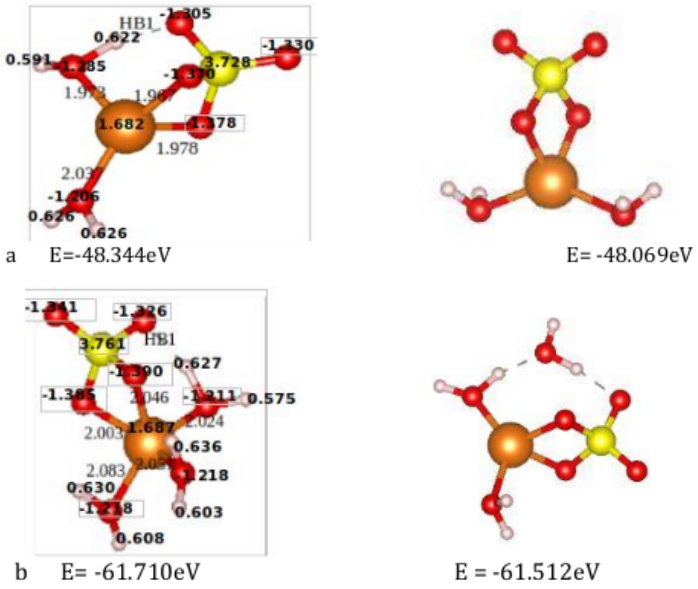

Figure 7: Bader charge and structural isomers of di hydrated $MgSO_4$ and tri-hydrated $MgSO_4$ with their corresponding Mg-O bond length (Å) and electronic energy

3.1.3 $MgSO_4$ .4H_2O and $MgSO_4$ .5H_2O

Figure 8a shows that, due to the increase in water molecules, there are now four hydrogen bonds (HB1, HB2, HB3, and HB4) are observed. As listed in table 1 below, hydrogen bonds like HB2 and HB3 in figure 9a below are on the weaker side of the hydrogen bond strength spectrum with O–O distances is found to be 2.706 and 2.705 Å respectively. The structure is formed with coordination number of four by equal two-two magnesium-oxygen bond length of 1.981 Å and 1.965 Å, as shown below. Two water molecules are directly linked with magnesium metal and the remaining two are stabilized by forming hydrogen bonds in both ends. The second structural isomer of Tetra-hydrated magnesium sulphate contains three hydrogen bonds: there and higher in electronic energy about 0.088 eV, and only one water molecule is stabilized by hydrogen bonding in both ends and the other three water molecules are coordinated with magnesium.

Another form of hydrated magnesium sulphate is penta-hydrated magnesium sulphate ($MgSO_4 \cdot 5H_2O$). Five water molecules encircle the magnesium sulphate compound in this hydrate. Water molecules in penta hydrated magnesium sulphate have the ability to create hydrogen bonds with one another. One water molecule's oxygen atom can form a hydrogen bond with another water molecule's hydrogen atom. The hydrate is more stable overall because of its network of hydrogen connections. The sulphate ions SO_4^{2-} in penta hydrated

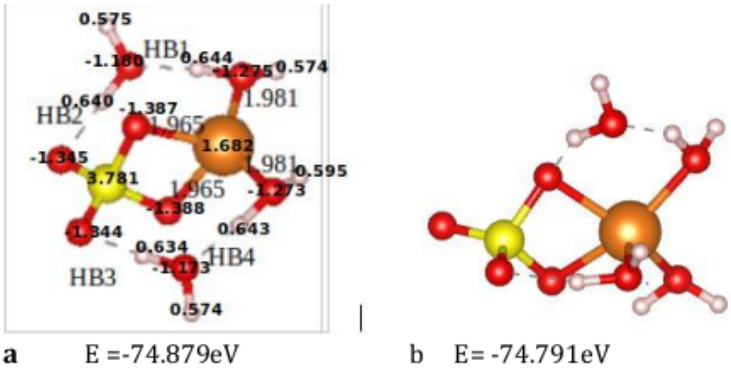

Figure 8: structural isomers of tetra-hydrated $MgSO_4$ with the corresponding Mg-O bond length (Å)

magnesium sulphate have a negative charged oxygen atoms. The $MgSO_4 \cdot 5H_2O$ optimized structure is shown in Figure 9. The structure contains three hydrogen bonds (HB1-HB3) with different O-H lengths. Since If each O-O bond length is greater than 2.6 Å, it is possible that they may not all fall into the strong hydrogen bond group.

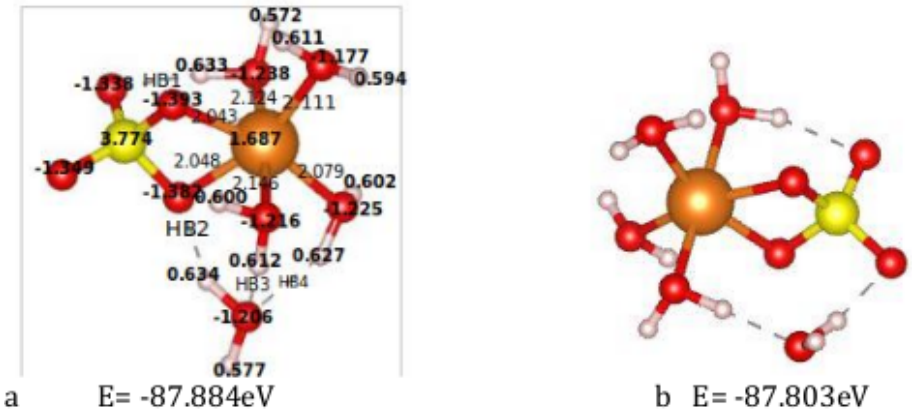

Figure 9: Bader charge and structural isomers of penta hydrated $MgSO_4$ with the corresponding Mg-O bond length (Å)

3.1.4 $MgSO_4 \cdot 6H_2O$

We have found two stable configurations for $MgSO_4 \cdot 6H_2O$, with an energy difference of 11.867 kJ/mol. Moreover, when two Oxygen atoms in the sulfate group bind with Mg, stability of the structural isomer increases with the one-oxygen-sulfur linkage. The first conformation depicted in Figure 10a is when one oxygen-sulfur atom is bound. with magnesium atom in this conformation, Mg coordinates five water molecules, while hydrogen bond formation stabilizes the one remaining water molecule. The conformation contains six hydrogen bonds and two of them (HB1 and HB6) meet the criteria for strong hydrogen bonds as defined in the previous section. But some studies show as all hydrogen bonds in

hexahydrate, none of them strictly meet the criteria to be strong hydrogen bond, which is disproved by our work [14].

The coordination sphere has an average atom of Mg and O is separated by 2.104 Å. The second structural isomer of hexa-hydrated magnesium sulfate is formed when two oxygen-sulfur atoms bind with magnesium atoms. In this conformation, Mg coordinates four water molecules, while hydrogen bond formation stabilizes the two remaining water molecules. In this study, the configuration contains five hydrogen bonds in all, and none of them strictly meets the criteria to be strong. The bond length of this type of isomer is slightly higher than that of the first structural isomer. The number of hydrogen bond formed is also decreased by one in the second structural isomers and this is due to the coordination of two Mg-O-S atoms in it, which is more stable than the first.

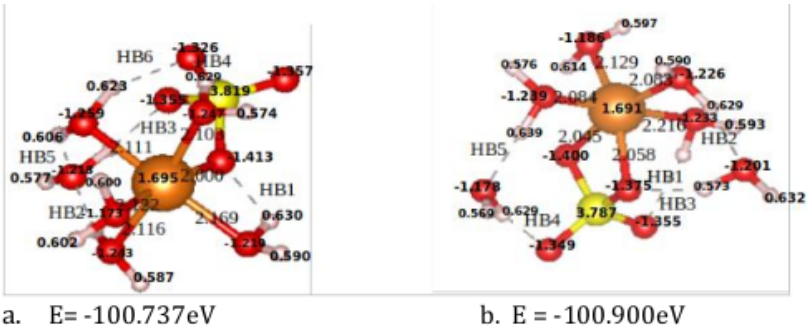

Figure 10: Bader charge and structural isomers of hexa-hydrated $MgSO_4$ with their corresponding Mg-O bond length (Å)

3.1.5 $MgSO_4$ .7H_2O

The heptahydrate form of magnesium sulphate contains seven water molecules per formula unit. Its molecular structure consists of one magnesium ion (Mg^{2+}) bonded to one sulphate ion (SO_4^{2-}) and seven water molecules. Two structural isomers were also selected for hepta hydrated magnesium sulphate. When one-oxygen atom in the sulfate group binds with the magnesium atom, and seven hydrogen bonds are formed with a coordination number of six around magnesium. In this case, two water molecules are stabilized by hydrogen bonds, as shown in figure 11a below. On the other hand, when two oxygen atoms in the sulfate group bind with the magnesium atom, the structure is formed by six hydrogen bonds with six coordinated magnesium and three water molecules are stabilized by hydrogen bonds (HB1, HB2, HB3, HB4, HB5 and HB6). The oxygen –sulfur length in each hydrogen bond is roughly equal, which is an average of 2.668 Å and magnesium-oxygen bond lengths is

also higher in this case.

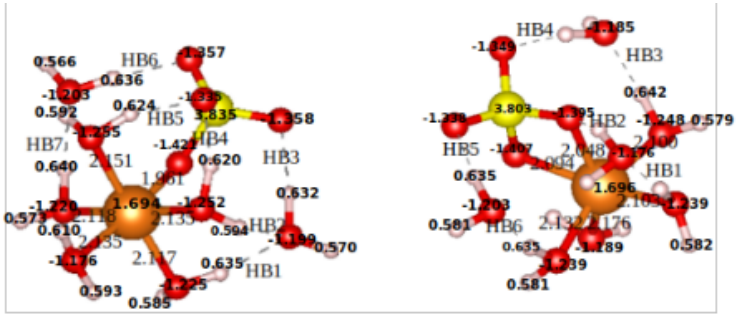

Figure 11: Bader charge and structural isomers of hepta hydrated $MgSO_4$ with their corresponding Mg-O bond length (Å)

3.1.6 $(MgSO_4)_2 \cdot nH_2O$

If the number of magnesium sulphate units in hydrated magnesium sulphate increases, from one to two, it would significantly impact the structure of the compound and it denotes a connection between two magnesium sulphate units, as shown in figures 12 a, b, and c. These bigger components would be arranged to create the final structure, which might resemble a more intricate lattice. Figure 12b is $(MgSO_4)_2 \cdot H_2O$ which is built from two $MgSO_4$ units linked together and one water molecule. Two-oxygen in two-sulfate groups are intermediate between two magnesium and sulphur atoms in the structure.

One hydrogen bond is observed in the structure of $(MgSO_4)_2.3H_2O$ shown in figure 12c. When the degree of As hydration increases, the number of hydrogen bonds to be created also increases. For example $(MgSO_4)_2.12H_2O$ contains 15 hydrogen bonds, as shown in Figure 12e. As the degree of hydration increases, the stability also increases because of the formation of multiple hydrogen bonds that decrease the electronic energy.

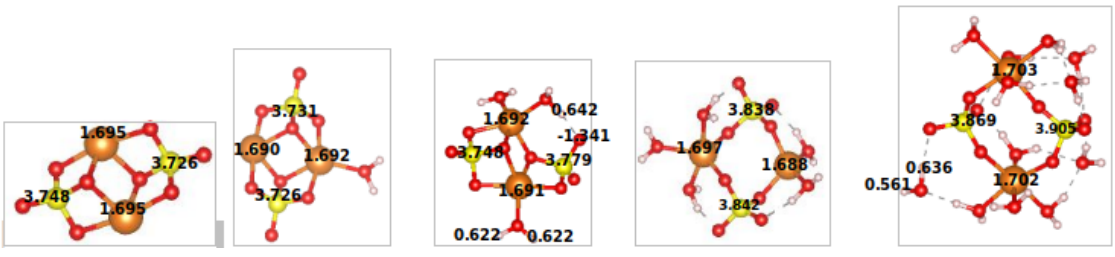

Figure 12: 12a–12e are the structures of different hydrated magnesium sulfate when the cluster size increases to two

3.2 Some possible structures of higher hydrates of magnesium sulphate and their hydrogen bonds

3.2.1 Structures of $MgSO_4$. $7H_2O$ type I

Depending on the coordination of magnesium with the sulfate group, we can subdivide the structures of hexa and hepta-hydrated magnesium sulfate as type I, when only one- oxygen of the sulfate group is linked with magnesium and type II, when two oxygen atoms are linked with magnesium, as mentioned before. There are three possible structural isomers of $MgSO_4.7H_2O$ type I with 8, 7 and 6 hydrogen bonds in their structures, as shown in figures 13a, 13b, and 13c, respectively. Among them are one that contains higher number of hydrogen bonds (Figure 13a) is more stable than the other with electronic energy of -113.812 eV.

In each of the three structures of figure 13a, 13b and 13c only two water molecules are stabilized by hydrogen bonds and the rest are coordinated with magnesium atom. The electronic energy difference between isomers having 7 hydrogen bonds in figure 13b and 6 hydrogen bonds in figure 13c is about 0.095eV. Another important thing from this kind of case is that the energy needed to remove water molecules from structures that have more hydrogen bond are also increased and this is because of hydrogen bond makes stability of that structure.

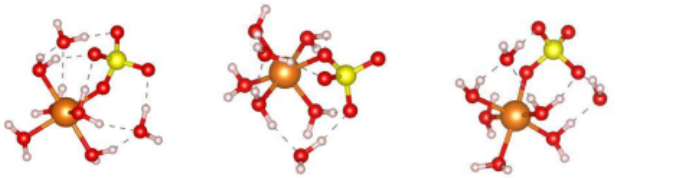

Figure 13: different structures of type I $MgSO_4.7H_2O$ with a) 8 b) 7 and c) 6 hydrogen bonds

3.2.2 Structures of $MgSO_4$. $7H_2O$ type II

The second type of structural isomer is when two oxygen atoms of the sulfate group are linked with magnesium atom in hepta-hydrated magnesium sulfate, which also contains two different structures that have 6 and 7 hydrogen bonds with electronic energy of -113.836 eV and -113.715 eV, respectively, in figures 14a and 14b. Similarly, the structure that

contains more hydrogen bonds and is relatively stable. Unlike type I structures, three water molecules are stabilized by hydrogen bonding in type II structural isomers. The coordination number of magnesium in both cases is six and out of them, four are water molecules around magnesium atom.

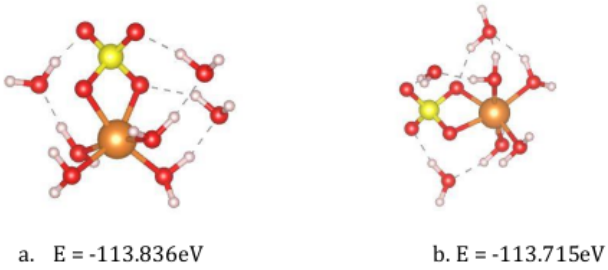

Figure 14: two different structures of type II $MgSO_4.7H_2O$ with a) 6 and b) 7 hydrogen bonds

3.2.3 Structures of $MgSO_4$. $6H_2O$ type I

In hexa-hydrated magnesium sulphate, two types of isomers are also identified with different hydrogen bonding based on the linkage of oxygen atoms in the sulfate group to magnesium atom. When one oxygen atom of the sulfate group binds with magnesium atom, then it is considered as type I and there are three structures with 4, 5 and 6 hydrogen bonds as shown in the figure below. Among the three types of isomers, the one with 6 hydrogen bonding (figure 15a) is relatively stable and contains minimum electronic energy, which is equal to -100.738 eV. The structure of hexa hydrated magnesium sulphate with 5 hydrogen Bonding is the second possible isomer that has -100.675 eV electronic energy, and so on.

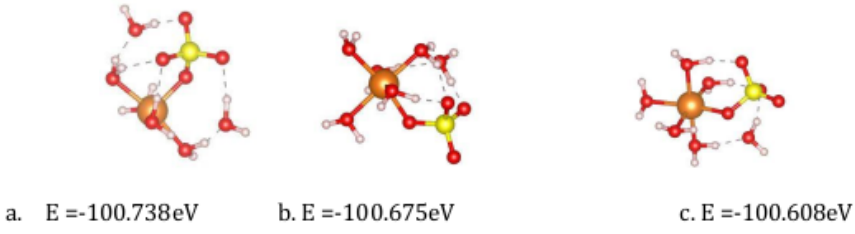

Figure 15: three possible structures of type I $MgSO_4.6H_2O$ with different hydrogen bond formation

3.2.4 Structures of $MgSO_4$. $6H_2O$ type II

There are two structural isomers of type II $MgSO_4.6H_2O$ that have hydrogen bond of 4 and 5 in two cases. The electronic energy difference between the two isomer is about -0.070 eV. In Contrary to the previous observation in hepta-hydrated case, the structure of hexa hydrated magnesium sulphate is stable with lower number of hydrogen bonds, which may caused by interaction of ions in it.

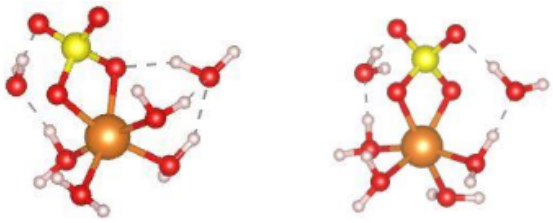

Figure 16: two possible structural isomers of type II $MgSO_4.6H_2O$ with a) 4 and b) 5 hydrogen bond formation

3.3 structures of hydrated magnesium sulfate that experience proton transfer

Since the sulfate ions (SO_4^{2-}) in hydrated magnesium sulfate can function as Lewis bases, they may be able to accept a proton from water molecules. Numerous factors influence this proton transfer (PT), which might happen under specific circumstances. The Lewis acid-base interaction is responsible for the proton's transfer from water to the sulfate ion. As a Lewis base, the sulfate ion can take up a proton (H^+) from a donor species due to its lone pairs of electrons on oxygen atoms. The relative acid-base strengths of the species involved affect the probability of proton transfer from water to sulfate ions. Hydronium and hydrogen sulfate ions can thus be formed when the sulfate ion accepts a proton from water under the right circumstances and all these hypotheses are also supported by Bader charge analysis. The solvation effect (hydrogen bonds) is fundamental for describing standard $MgSO_4$ systems. Solvation increases the Mg-S, OS-H and HW-O distances due to the hydrogen bond, thus avoiding the PT process [48]. In the case of hexa- and hepta-hydrated magnesium sulfate, we prepare the cluster manually from bulk structure to have an exact representation of the bulk. But, during optimization, there is also a proton transfer in both

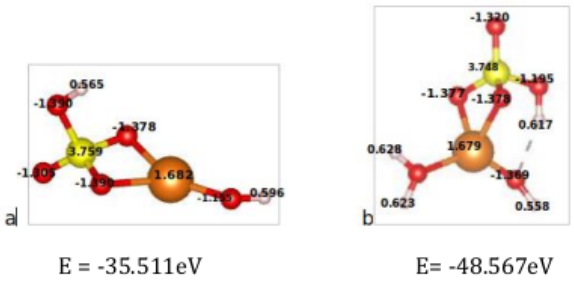

E = -35.511eV E= -48.567eV

Figure 17: Bader charge, structure and energy of a) monohydrated $MgSO_4$ and b) dihydrated $MgSO_4$ that involves in proton transfer with the corresponding Mg-O bond length (Å)

hexa- and hepta-hydrated magnesium sulfate, and this may be due to one of the above reasons, which is also supported by the investigation of bader charge analysis. The bulk structure of hepta and hexa hydarates are not the same as that of lower hydrates. In the case of higher hydrates, $n \geq 6$, all water molecules are coordinated with the magnesium atom, the sulfate group and any more water molecules are stabilized by the formation of hydrogen bonds. There are also more than four hydrogen bonds, as shown in the following figures, including the length of the O-O bond less than or equal to 2.5 Å, which are considered as hydrogen bonds according to Jeffery.

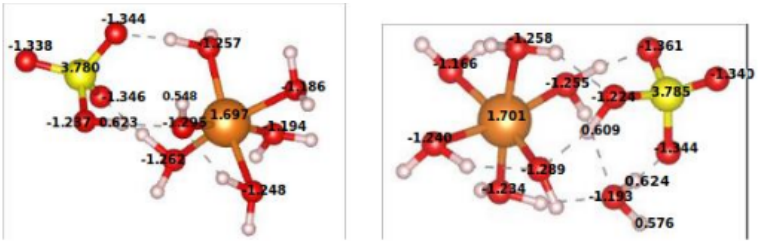

a. E =-100.189eV b. E =-113.045eV

Figure 18: structures of hexa- and hepta hydrated magnesium sulphate in which proton transfer takes place.

3.4 Hydrogen bonds in the $MgSO_4$ hydrate system

Due to the interaction between water molecules and magnesium sulfate ions in the crystal lattice, the electrical energy of hydrated magnesium sulfate increases with increasing hydration. Water molecules attach themselves to the sulfate ions and/or other water molecules in the hydrate by hydrogen bonding. The positively charged hydrogen atoms in water molecules and the negatively charged oxygen atoms in sulfate ions interact electrostatically to form these hydrogen bonds [12]. As we can see clearly from table 1, the number of

hydrogen bond increases with increasing degree of hydration. The electronic energy of higher hydrates is also smaller than that of lower hydrates, which means that stability increases with an increasing hydrogen bond.Table 1 below contains all the bond length of O—H, O–H, and O—O and bond angle of OHO bents. Depending on Jeffery, we can classify hydrogen bonds as strong, moderate, or weak. The bond angle of $\angle OHO$ is between $140.823^{o} - 175.181^{o}$, which is good agreement with previous study [48].

molecule	Coord. number (CN)	hydrogen bond name (HB)	O-H (Å)	$\mathbf{H}\cdots$O(Å)	0 – 0(Å)	∠OHO (deg)
$MgSO_4 \cdot 2H_2O$	4	HB1	1.003	1.998	2.931	153.559
$MgSO_4 \cdot 3H_2O$	5	HB1	1.067	1.517	2.554	162.195
$MgSO_4.4H_2O$	4	HB1	1.053	1.510	2.558	172.294
		HB2	1.013	1.700	2.706	171.399
		HB3	1.006	1.706	2.705	171.111
		HB4	1.054	1.508	2.556	172.281
$MgSO_4 \cdot 5H_2O$	6	HB1	0.995	1.858	2.757	148.742
		HB2	0.987	1.947	2.789	141.562
		HB3	1.013	1.650	2.581	150.607
		HB4	1.018	1.742	2.712	157.611
$MgSO_4 \cdot 6H_2O$	6	HB1	0.990	1.914	2.553	119.683
(type-1)		HB2	1.009	1.666	2.642	161.689
		HB3	1.034	1.554	2.582	171.783
		HB4	1.008	1.748	2.665	149.274
		HB5	0.983	1.980	2.811	140.823
		HB6	1.041	1.556	2.548	157.529
$MgSO_4 \cdot 6H_2O$	5	HB1	0.988	1.951	2.865	152.666
(type-2)		HB2	1.002	1.739	2.688	152.542
		HB3	1.007	1.702	2.635	152.180
		HB4	1.001	1.785	2.776	169.551
		HB5	1.022	1.626	2.646	175.181
$MgSO_4 \cdot 7H_2O$	7	HB1	1.002	1.762	2.732	161.597
(type-1)		HB2	0.982	2.065	2.887	140.051
		HB3	1.012	1.718	2.722	170.636
		HB4	1.012	1.701	2.646	153.558
		HB5	1.017	1.672	2.630	155.212
		HB6	1.011	1.723	2.730	170.938
		HB7	1.001	1.785	2.743	158.927
$MgSO_4 \cdot 7H_2O$	6	HB1	1.020	1.655	2.655	165.568
(type-2)		HB2	0.993	1.805	2.690	146.522
		HB3	1.021	1.612	2.628	173.337
		HB4	1.007	1.696	2.695	170.773
		HB5	1.010	1.662	2.661	168.699
		HB6	1.008	1.685	2.678	167.465

Table 1: Hydrogen Bond Parameters in the Conformations

3.5 Vibrational Frequency calculation

The stability of a substance or a crystal structure can be determined by the vibrational frequencies.All vibrational frequencies in a stable structure should have real values.This suggesting that the system is in a minimum-energy configuration. In contrast, imaginary frequencies imply that the structure is dynamically unstable and subject to phase transitions or structural deformation. By examining the second derivatives of the total energy with respect to atomic displacements, vibrational frequencies can be computed [49].

The exchange-correlation functional has an impact on these second derivatives, which are sometimes referred to as force constants or Hessian matrix elements. Variations in the force constants can have an impact on the computed vibrational frequencies because different exchange-correlation functionals describe electron-electron interactions differently. Magnesium sulfate hydrates, such as magnesium sulphate heptahydrate ($MgSO_4 \cdot 7H_2O$), can have lower vibrational frequencies for a variety of reasons. Water molecules usually form hydrogen bonds with the ions or molecules around them in hydrated environments. By changing the binding strengths and exerting influence on nearby atoms, hydrogen bonds have the ability to modify vibrational frequencies.

Vibrational frequencies may drop as a result of changes in the hydrogen bonding network caused by a decrease in the quantity of water molecules around the magnesium sulphate. Magnesium sulphate hydrates' crystal structure has a variable quantity of water molecules depending on variations in humidity, pressure, and temperature. The overall structure of the crystal may change if water molecules are taken out of the lattice. Vibrational frequencies may drop as a result of these structural changes, which may also change binding strengths, force constants, and interatomic distances. Additional intermolecular interactions, such as dipole-dipole interactions and van der Waals forces, may be introduced into the crystal structure by the presence of water molecules. Through modifications to the system's potential energy surface, these interactions can have an impact on vibrational frequencies. The strength and kind of these intermolecular interactions can alter in the absence of water molecules, which lowers vibrational frequencies.

The provided plot in figure 19 compares the vibrational frequencies of the sulfate ion (SO_4^{2-}) as found by actual observations with those obtained from Molecular Dynamics (MD) simulations. The degree of hydration is indicated by the x axis, which shows the number of water molecules per unit of formula, and the y axis, which displays the vibrational

No	hydrates	$\nu_1^{SO_4^{2-}}\left(cm^{-1}\right)$, This work/expt [50]			
		symmetric stretching (ν_1)	asymmetric stretching (ν_3)	bending modes (ν_2/ν_4)	Experimental (ν_1)
1	$MgSO_4 \cdot 7H_2O$_s1	987.61	1067.3	632.77-421.32	984.7±0.3
2	$MgSO_4 \cdot 7H_2O$_s2	982.8	1009.34	668.84-440.16	–
3	$MgSO_4 \cdot 6H_2O$_s1	984.65	1010.6	769.28-499.00	984.5 ±0.3
4	$MgSO_4 \cdot 6H_2O$_s2	969.6	1048.26	647.75-463.10	–
5	$MgSO_4 \cdot 5H_2O$	1002.3	1025.15	663.21 - 478.37	1004.9
6	$MgSO_4 \cdot 4H_2O$	998.7	1055.58	708.48 -519.64	1000.5
7	$MgSO_4 \cdot 3H_2O$	1009.8	1137.63	677.24 - 466.41	1023.8
8	$MgSO_4 \cdot 2H_2O$	1016.2	1254.59	773.512 -459.02	1033.8
9	$MgSO_4 \cdot 1H_2O$	1023.4	1111.03	764.98 - 448.72	1043.5 - 1046.1
10	$(MgSO_4)_2 \cdot 1H_2O$	996.68	1256.46	654.07-485.27	–
11	$MgSO_4$	1065.7	1253.63	734.31 - 554.58	1052.7

Table 2: Vibrational frequencies of sulfate ions in hydrated magnesium sulfate.

frequencies in cm^-1. Both the theoretical simulation and the actual experimental data from the literature show a general trend of decreasing vibrational frequency with increasing hydration content, with slight variability. The simulation data begins at a frequency higher than the experimental data for zero water molecules, crosses over to one and two water molecules, and then continues in a similar pattern for the rest of the plot, even at a frequency lower than the experimental values.

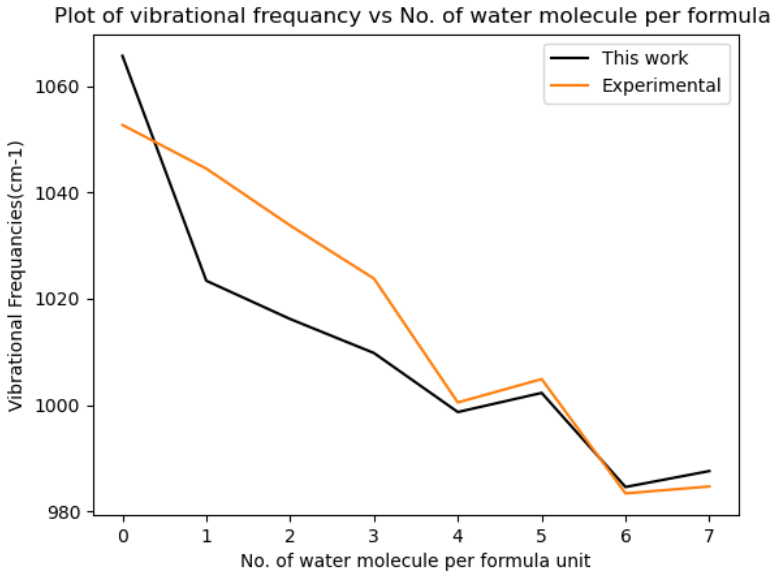

Figure 19: Plot of vibretional frequency vs number of water molecule per formula unit

3.6 Equilibrium product Expression of dehydration of $MgSO_4.nH_2O$

The ΔG of a system depends on its parameters, including temperature, pressure, and other factors. The ΔG (from equation (13)) should be zero in chemical equilibrium, providing information about the equilibrium concentration of products.The dehydration curve typically shows distinct stages or steps corresponding to the removal of water molecules from the hydrates. For example, in the case of magnesium sulfate hepta hydrate ($MgSO_4 \cdot 7H_2O$), the curve may show multiple steps corresponding to the sequential loss of water molecules. Each step represents a different hydrate or an intermediate phase. The different steps on the curve correspond to different temperatures at which specific hydrates or intermediate phases lose water. By analyzing the curve, we can determine the temperatures required for the dehydration of each hydrate.

Lower hydrates, such as monohydrate or dihydrate, have more closely linked water molecules due to hydrogen bonding with the magnesium sulfate ions and one another, higher ionic interaction. These hydrates have relatively stable crystal lattice structures, and more energy is needed to break the bonds that hold the water molecules and ions together. In higher hydrates, such as hexa hydrate or more, the bonding forces weaken and the stability of the crystal lattice is reduced as the number of water molecules drops. As a result, these hydrates can undergo dehydration at a lower temperature than the lower hydrates.

3.6.1 Dehydration reaction of $MgSO_4$ hydrates

Hydrate molecules absorb heat energy during the endothermic process of dehydration which causes them to break down into lower-hydrate or anhydrous forms. The equilibrium products of the dehydration reaction are examined in the temperature range of 290 to 995 K in order to comprehend the impact of temperature on the dehydration reaction of $MgSO_4$ hydrates. All that is manipulated in the experimental dehydration setup are the pressures of water vapor, P_{H2O}.

The partial pressure of the hydrates is kept constant at 1atm in the current study, whereas the control variables are the system temperature and the partial pressure of the water. For all dehydration reactions involving hydrates of magnesium sulfate, the equilibrium water vapor pressure is dependent on the system temperature. For compact seasonal heat storage, magnesium sulphate heptahydrate $MgSO_4.7H_2O$ was studied as a possible TCM [51]. The energy needed to extract water molecules from a molecule or an ion is known as the

dehydration energy, and it can provide information on the strength of ionic and hydrogen bonding interactions between molecules.Therefore, understanding the stability and behavior of molecules in a variety of chemical and biological processes requires knowledge of this information. According to Equation 19 stated in Section 2.3, the dehydration energy of higher hydrates is easier than that of lower hydrates, and this finding is also supported by our dehydration curve shown in the next section. The calculated dehydration energy of heptahydrated magnesium sulfate is -25.705 eV per mole of water, while removing one water molecule from monohydrated magnesium sulfate requires more energy and the dehydration energy is found to be -184.936 eV. According to experiments, there are multiple dehydration processes involved in the second phase, most likely including an ($MgSO_4 \cdot 2H_2O$) intermediate, and due to this, we are include the dehydration of some hydrates, like tetrahydrate and dihydrates.

The second dehydration process involves a material structure transition from crystalline ($MgSO_4 \cdot 6H_2O$) to an amorphous phase until crystalline $MgSO_4$ is created, according to X-ray diffraction measurements [13]. We are interested in plot the dehydration curve of the above reactions and some additional dehydration curves for further investigation, as follows:

3.6.2 Dehydration curve of $MgSO_4.7H_2O$ to $MgSO_4.6H_2O$ and $MgSO_4.5H_2O$ to lower cases

Dehydration curve helps in understanding the transformation of hydrates into anhydrous compounds and provides insights into the physical and chemical properties of magnesium sulfate in different hydration states. Our finding shows that the dehydration of higher hydrates happens at lower temperatures and vice versa for lower hydrates, which is in line with experimental findings. In Figure 20, the equilibrium water vapour pressure in relation to temperature is displayed for each of the dehydration reactions (from hepta hydrated to hexa hydrate, and hepta to penta hydrated, and to lower case).

The partial pressures of the hydrates are held constant at 1 atm throughout this computation, and only the partial pressure of H_2O is changed. In the dehydration curve plotted below, the isomer that is identified in terms of the bond between magnesium and one oxygen-sulfur isomer (7-1SO) dehydrates at lower temperature than the second isomer of two oxygen-sulfur atoms linked with one magnesium atom (7-2SO), as shown in the

following figure. The growing instability of these hydrates with rising hydration number can be the reason for the dehydration of higher hydrates, which starts at lower temperatures. Water molecules are integrated into the compound's crystal lattice during the formation of a hydrate. Intermolecular forces, such as hydrogen bonds, stabilize the hydrate structure and hold the water molecules in place. Nevertheless, the stability of these intermolecular forces decreases with an increase in the amount of water molecules per formula unit.

The one-set computational temperature for the dehydration of $MgSO_4.7H_2O$, 7-1SO to $MgSO_4.6H_2O$, 6-2SO is around 290K, which is in good agreement with the experimental finding as mentioned in the introduction section of this study. Dehydrating $MgSO_4.7H_2O$ (when 2 S-O atoms are bonded with magnesium) to ($MgSO_4.6H_2O$) (when 1 S-O atoms is bonded to magnesium), it requires a higher temperature than dehydrating ($MgSO_4.7H_2O$) when 2 S-O atoms are bonded with magnesium to ($MgSO_4.6H_2O$) when 2 S-O atoms are bonded with magnesium, as shown in figure below. Removing four water molecules and

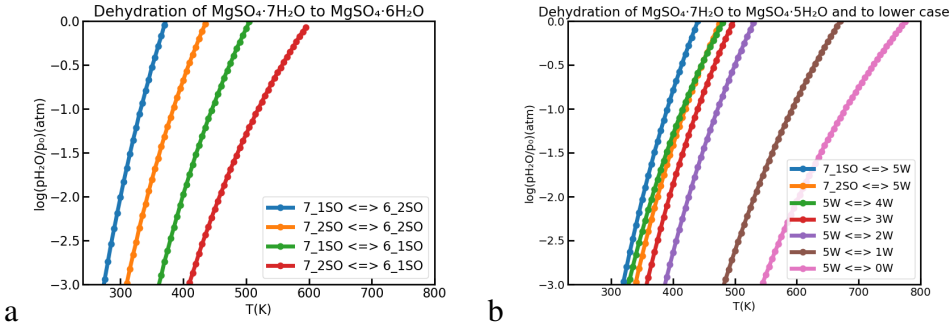

a b

Figure 20: Equilibrium vapor pressure for the dehydration reactions of $MgSO_4.7H_2O$ and$MgSO_4.5H_2O$ hydrates at various temperatures and constant partial pressure of hydrate, p^o = 1 atm

all water from penta hydrated magnesium Sulfate starts to escape out with a computational temperature above 490K, which is far from other dehydration-onset temperatures of penta-hydrated magnesium sulphate. This is also the effect of a strong ionic bond in the lower-hydrated case. In conclusion, higher hydrates can dehydrate more easily at lower temperatures because of the decreased stability of the hydrate structure as the hydration number increases and the greater porosity of the crystal lattice, which facilitates the escape of the water molecule.

3.6.3 Dehydration curve of $MgSO_4$. $6H_2O$ to lower hydrates and tetrahydrate to lower hydrate

The higher hydrate absorbs energy and breaks down into smaller hydrates and H_2O molecules during the dehydration phase. As the temperature increases from 305 K to 400 K, the dehydration of the hydrated salt, $MgSO_4.6H_2O$, is fast and four water molecules are released at this stage.As we can see clearly from the figure below, removing one water molecule requires a higher temperature, and the gap between the curves is broader than the sequential dehydration of higher hydrates. The offset can result from the ideal polyatomic gas phase hypothesis.

Figure 21 demonstrates the influence of temperature on $MgSO_4.6H_2O$ and $MgSO_4.4H_2O$ in both cases the dehydration curve is consistent with the experiments [52]. The offset can result from the ideal polyatomic gas phase hypothesis. There is also a clear observation in the higher hydrates, which can easily dehydrate relatively at lower temperature and is consistent with the previous studies. However, a lower-hydrated magnesium sulfate requires a higher temperature, which is roughly above 450 K, and this may be due to the ionic bond between the Mg^{2+} and SO_4^{2-} ions, as demonstrated in Figures 21a and 21b.

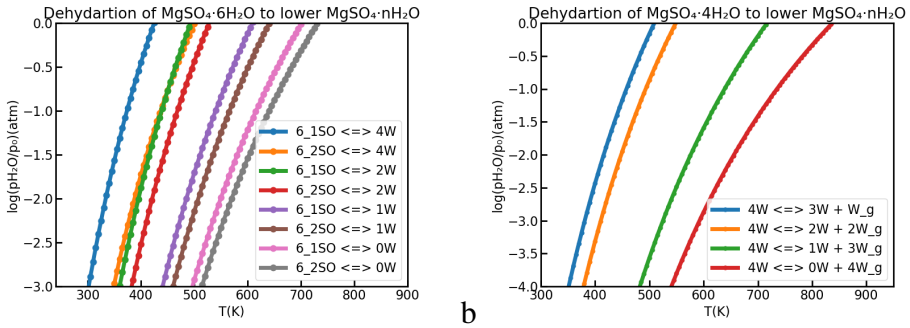

a b

Figure 21: Equilibrium vapor pressure for the dehydration reactions of a) $MgSO_4.6H_2O$ b) $MgSO_4.4H_2O$ hydrates to lower hydrates at various temperatures and constant partial pressure, $p^o = 1$ atm

3.6.4 Dehydration curve of $MgSO_4$. $2H_2O$ to $MgSO_4 \cdot H_2O$ and $MgSO_4$

In similar manner, if there are lower hydrates, then the ionic interactions increase and the onset temperature also increase. The dehydration of $MgSO_4.2H_2O$ and $MgSO_4 \cdot H_2O$ two anhydrous occurs at a higher temperature than any hydrate of magnesium sulfate and this is because the ionic interaction is higher than other hydrates.

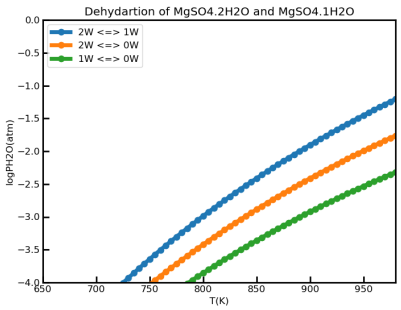

Figure 22: Equilibrium vapor pressure for the dehydration reactions of $MgSO_4.2H_2O$ hydrates to $MgSO_4.H_2O$ and $MgSO_4$ at various temperatures and constant partial pressure, p^o = 1 atm.

3.6.5 Dehydration curve of non-stoichiometric magnesium sulfate hydrates

In contrast to higher hydrates like the heptahydrate ($MgSO_4 \cdot 7H_2O$), lower hydrates of magnesium sulfate, such as the monohydrate ($MgSO_4 \cdot H_2O$) or less than monohydrates ($MgSO_4 \cdot nH_2O$), where n is between zero and one, generally requires higher temperatures during dehydration. There are several explanations, and the first one is in comparison to higher hydrates and lower hydrates contain fewer bonding interactions between magnesium sulfate ions and water molecules and a higher ionic interaction [53]. Therefore, in in order to break the hydrogen bonds binding the water molecules within the crystal structure, more thermal energy is needed to overcome these weaker bonds.

The second reason may be that the crystal structures of lower hydrates are frequently more stable and compact than those of higher hydrates due to ionic interaction between magnesium and sulphate ions [52]. The hydrate's stability is increased by the closely spaced arrangement of water molecules inside the crystal lattice. Higher temperatures are required to break up this stable arrangement and liberate the water molecules.

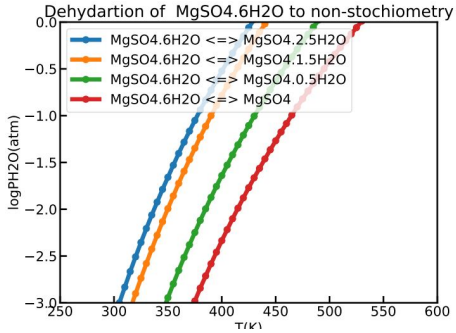

Figure 23: Equilibrium vapor pressure for the dehydration reactions of $MgSO_4.6H_2O$ hydrates to fractional water molecules.

3.6.6 Computational values of Thermodynamic properties and the corresponding Experimental Values

Understanding the thermochemical behavior of hydrated magnesium sulfate requires an understanding of equation 13. We can forecast the Gibbs free energy change (Δ G) of various hydrated magnesium sulfate compositions and ascertain their suitability for thermochemical energy storage by examining the changes in entropy (ΔS) and enthalpy (ΔH) during the hydration/dehydration reactions. This makes it possible to find compositions that have good thermal stability and energy storage capacity.

$$\Delta G = \Delta H - T\Delta S \tag{27}$$

Table 3 below shows the calculated dehydration energies (Δ_{deh}E and $\Delta_{deh}E$+ZPE), dehydration enthalpy ($\Delta_{deh}H$), and dehydration Gibbs Free Energy ($\Delta_{deh}G$) for the dehydration reactions of $MgSO_4.7H_2O$ to $MgSO_4.6H_2O$. All values are expressed in kJ / mol of H_2O. $\Delta_{deh}E$ denotes the dehydration energies calculated using the electronic energy of DFT, corresponding to T = 0K and p = 1 atm. $\Delta_{deh}E$+ZPE denotes the dehydration energies in which zero-point energy corrections are included in $\Delta_{deh}E$. The last two columns, namely ($\Delta_{deh}H$) and $\Delta_{deh}G$, are calculated at 25°C and p = 1 atm. Depending on the particular hydrate and the circumstances surrounding the interaction, the reaction enthalpies of magnesium sulphate hydrates, which indicate the heat generated or absorbed during their production or decomposition can change [54]. We have considered the structure to have minimum energy while calculating reaction enthalpies. For each of the hydrates under study, When the number of hydrations increases from 1 to 7, the dehydration enthalpy emitted per H_2O molecule drops .This implies that electrostatic attraction might be the dominant factor influencing the dehydration enthalpy. It is simpler to dehydrate two H_2O molecules from $MgSO_4.7H_2O$ than it is to remove the same two H_2O molecules from $MgSO_4.6H_2O$ and so on.

$$MgSO_4.7H_2O + \Delta X \rightleftharpoons MgSO_4.6H_2O + 1H_2O \tag{28}$$

Where X = E, E+ZPE, H, and G. St1 indicates when one oxygen-sulfur atom is connected to magnesium, and St2 is also when two oxygen-sulfur atoms are connected to magnesium for both hepta and hexa hydrates.VASP optimization also has the best agreement in computational energetics with experimental value energetics with offset values of ±2 and a

maximum temperature offset value of $\pm 12K$ for structure 2, and this may come from the approximation used in optimizing structures.

No	Dehyd. Rxn	$\Delta_{deh}E$	$\Delta_{deh}E$ +ZPE	$\Delta_{deh}H$	$\Delta_{deh}G$	$T_{min}/T_{max}(K)$	-TΔS (KJ / mol)
1	$MgSO_4.7H_2O$ st2 $\rightleftharpoons$ $MgSO_4.6H_2O$ st2 + H_2O	66.482	57.430	61.200	19.130	305/400	41.823
2	$MgSO_4.7H_2O$ st2 $\rightleftharpoons$ $MgSO_4.6H_2O$ st1 + H_2O	84.437	72.730	65.850	27.250	405/500	37.734
3	$MgSO_4.7H_2O$ st1 $\rightleftharpoons$ $MgSO_4.6H_2O$ st2 + H_2O	65.421	54.230	59.300	11.530	380/490	47.486
4	$MgSO_4.7H_2O$ st1 $\rightleftharpoons$ $MgSO_4.6H_2O$ st1+ H_2O	72.971	86.320	63.210	20.40	290/320	43.396
	Experimental value [55]			62.740	10.020	298/328	
5	$MgSO_4.6H_2O$ st1 $\rightleftharpoons$ $MgSO_4.4H_2O$ + $2H_2O$	136.462	114.68	120.85	35.139	300/450	85.178
6	$MgSO_4.6H_2O$ st2 $\rightleftharpoons$ $MgSO_4.4H_2O$ + $2H_2O$	154.193	129.98	134.860	53.260	350/500	81.089
	Experimental value [55]			105.83	21.510	333/–	
7	$MgSO_4.4H_2O$ $\rightleftharpoons$ $MgSO_4.3H_2O$ + H_2O	90.856	80.06	86.17	35.590	395/365	50.270
	Experimental value [55]			46.580	46.580	–/–	
8	$MgSO_4.2H_2O$ $\rightleftharpoons$ $MgSO_4.H_2O$ + H_2O	155.424	153.140	74.35	113.610	> 650	37.951
	Experimental value [55]			42.460	–	> 530	–
9	$MgSO_4.H_2O$ $\rightleftharpoons$ $MgSO_4$ + H_2O	143.422	133.05	173.62	105.72	> 700	37.206
	Experimental value [55]			42.460	–	> 550	–

Table 3: Calculated Dehydration Energies, Dehydration Enthalpy, and Dehydration Gibbs Free Energy for the dehydration reactions of $MgSO_4.7H_2O$ and Other Lower hydrates.

3.7 Optimized Composite Structures of Magnesium sulfate Species using normal Si-O Frameworks

3.7.1 Impregnated $MgSO_4$ to FAU

Figures 24 and 25 depict the structure of an impregnated magnesium sulfate-FAU of the Si-O normal framework of composites at both the sodalite (Figure 25a) and alpha (Figure 25b) openings. In the sodalite cage, magnesium coordinates with oxygen from FAU in three directions, forming bonds with an average length of 2.180 angstrom. This composite exhibits an electronic energy of -1182.796 eV, and the adsorption energy is found to be -3.582 eV. The higher coordination number in the sodalite cage makes the composite more stable, providing valuable insights into the stable arrangement of magnesium sulfate within

the FAU framework at the sodalite opening.

The second structure shows cases of magnesium sulfate impregnated within the alpha cage of the FAU zeolite. The alpha cage, part of the three-dimensional network of interconnected cages and channels in the FAU zeolite, incorporates magnesium sulfate. Here, magnesium coordinates with two oxygen atoms of the FAU-zeolite framework. The electronic energy of this configuration is recorded as -1181.335 eV, and the calculated adsorption energy is –2.121 eV. A more negative adsorption energy typically indicates a stronger adsorption interaction between the adsorbate and the adsorbent. In the context of this, where electronic energies are mentioned, a more negative electronic energy suggests a more favorable or stronger adsorption [23].

The magnesium sulfate-FAU composite contains a large pore volume and high surface area, making it an excellent candidate for applications as an adsorbent, and, in this case, magnesium coordinates with two oxygen atoms in the FAU-zeolite framework, resulting in a bond length of around 2.140 angstrom, whereas in the sodalite cage, magnesium coordinates with FAU oxygen in three directions, indicating multiple coordination sites within the cage that make it more stable than alpha-impregnated $MgSO_4$ but this does not work for higher hydrates due to its small volume.

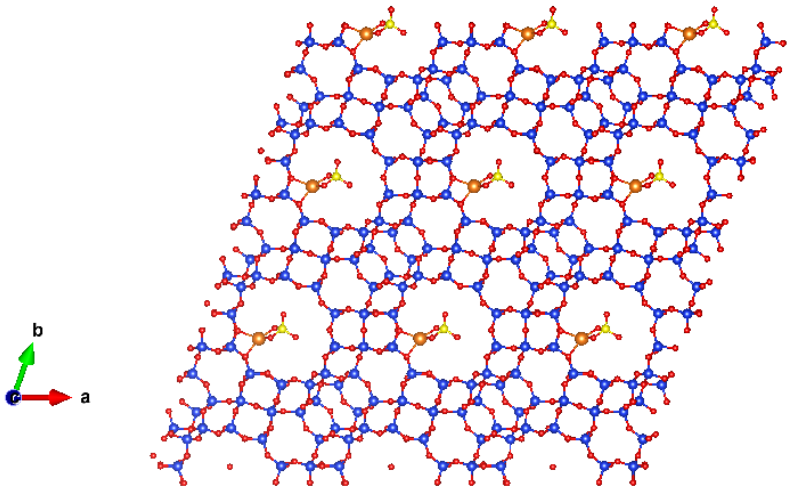

Figure 24: Magnesium sulfate at super cages in FAU zeolite

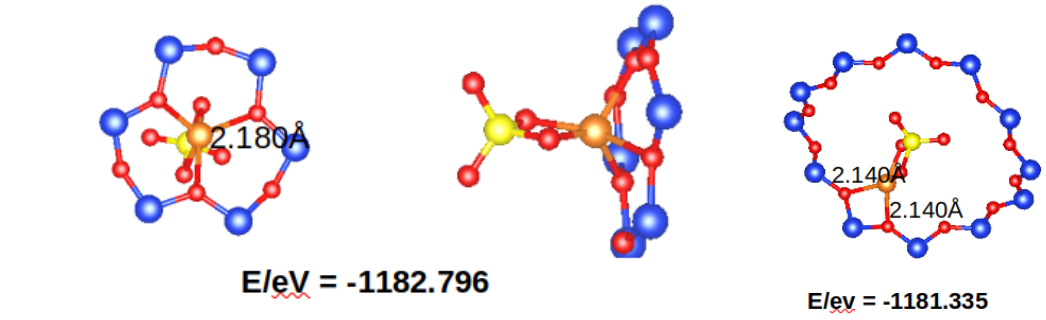

a b

Figure 25: Magnesium sulfate at a) sodalite and b) super cages in FAU normal Si-O zeolite

3.7.2 Impregnated $MgSO_4.H_2O$ to FAU

In the alpha-$MgSO_4.H_2O$ FAU composite structures, two possible isomeric structures exist with similar electronic energies. The first structural isomer forms a hydrogen bond with the FAU framework, with a bond length equal to 2.730Å, and the second isomer is derived from the anhydrous magnesium sulfate composite by incorporating one water molecule. In this type of isomer, coordination with the FAU framework occurs at two ends, with bond lengths of 2.180 Å and 2.220 Å, as depicted in Figure 26. The electronic energy of the first isomer is recorded as -1196.277 eV, while the second isomer has an electronic energy of -1196.921 eV. Higher electronic energy, mainly -1197.3360 eV, is also recorded in the sodalite opening for this type of composite structure, as shown in figure 27 below. The adsorption energy in the sodalite cage and super cage was found to be –1.964 eV.

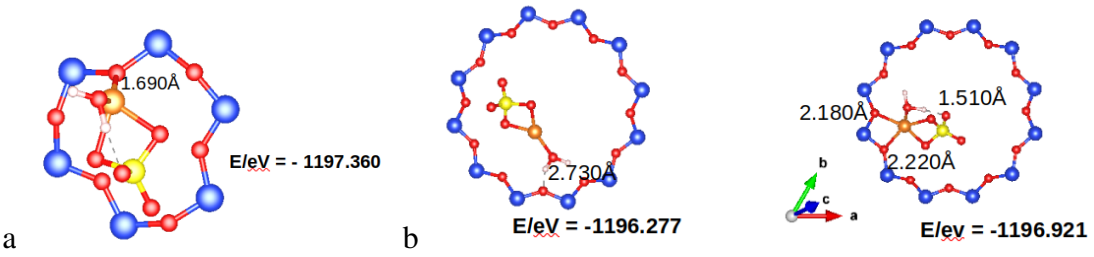

a b

Figure 26: Mono hydrated magnesium sulfate: a) atsodalite cage and b) two isomers of $MgSO_4.H_2O$ at super cages in FAU zeolite

3.7.3 Impregnated $MgSO_4.2H_2O$ and $MgSO_4.3H_2O$ to FAU

As the degree of hydration increases, incorporating hydrated magnesium sulfate into sodalite cages is impossible due to the small volume of it and would distort the FAU structures if it happened. Therefore, we incorporate higher hydrates only in alpha (super) cages due to their

large volume and ability to impregnate a large number of atoms. Two isomeric structures of dihydrated magnesium sulfate exhibit different coordination patterns of magnesium within the FAU framework. The first composite structure involves magnesium coordinated with the FAU framework with a bond length of 2.210 Å, accompanied by a hydrogen bond with a length of 1.940 Å to the FAU framework.

This isomer possesses an electronic energy of -1211.977 eV and –0.9394 eV of adsorption energy. The second isomer, on the other hand, features only one hydrogen bond measuring 1.960 Å and an electronic energy of -1211.842 eV. In the alpha-FAU structure, trihydrated magnesium forms two hydrogen bonds with O-H lengths of 1.671 Å each. The electronic energy of tri-hydrated magnesium sulfate-FAU is found to be -1227.311 eV and the adsorption energy is –1.054 eV which is slightly higher than the dihydrared magnesium sulfate-FAU adsorption energy.

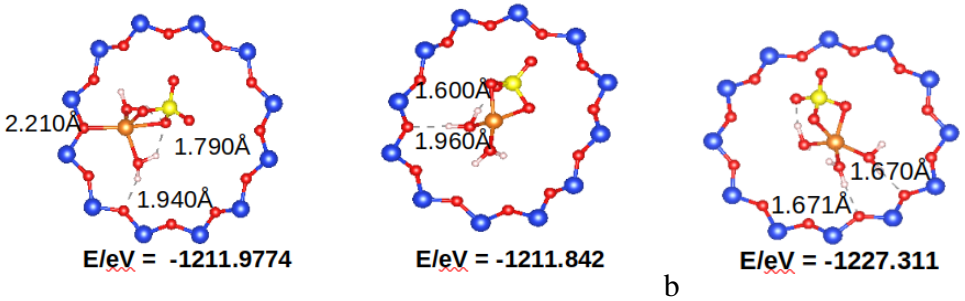

a b

Figure 27: a) Di-hydrated and b) Tri-hydrated magnesium sulfate at super cages in Si-O FAU zeolite

3.7.4 Impregnated $MgSO_4.4H_2O$ and $MgSO_4.5H_2O$ to FAU

Impregnating both tetra-hydrated $MgSO_4$ with an electronic energy of -1242.675 eV and penta-hydrated $MgSO_4$ with an electronic energy of -1257.346 eV into alpha-FAU zeolite produces some fascinating findings. The adsorption energies for these molecules are determined to be -1.265 eV and -0.859 eV, respectively, within the zeolite framework. This indicates a favorable interaction between the hydrated $MgSO_4$ species and the zeolite matrix. The negative adsorption energies suggest that the impregnation of both tetra and penta-hydrated $MgSO_4$ into the alpha FAU zeolite lattice is energetically advantageous, indicating strong binding between the $MgSO_4$ species and the zeolite framework. These findings provide valuable insights into the stability of the adsorbed species. Further exploration of the structural and electronic properties of these impregnated systems will indeed

contribute to advancing our understanding of zeolite-based materials and their diverse range of applications.

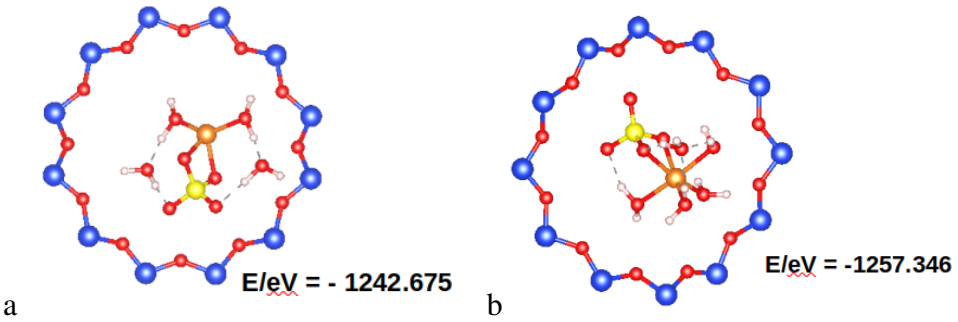

a b

Figure 28: a) Tetra-hydrated and b) penta-hydrated magnesium sulfate at super cages in FAU zeolite

3.7.5 Impregnated $MgSO_4.6H_2O$ and $MgSO_4.7H_2O$ to FAU

The impregnated hexa and hepta-hydrated $MgSO_4$ in FAU-zeolite may have potential applications in energy storage systems. The strong binding between the $MgSO_4$ species and the FAU-zeolite can enable the storage of energy-rich compounds, facilitating the development of advanced batteries or supercapacitors.The hexa-hydrated $MgSO_4$ with an electronic energy of -1272.787 eV and the hepta-hydrated $MgSO_4$ with an electronic energy of -1287.934 eV exhibit fascinating behavior when impregnated into alpha FAU zeolite. The adsorption energies for these molecules are determined to be -1.193 eV and -1.327 eV, respectively. The negative adsorption energies indicate a strong affinity between the hydrated $MgSO_4$ species and the zeolite framework. This suggests that the impregnation of hydrated hexa and hepta $MgSO_4$ in alpha FAU zeolite is energetically favorable, resulting in stable binding between the species $MgSO_4$ and the framework zeolite. Figure 29 shown below demonstrates the adsorbed hydrates in the FAU matrix, highlighting the favorable interaction between the hydrated $MgSO_4$ molecules and the zeolite lattice. These findings have significant implications for various applications such as catalysis, separation, and ion exchange, where the presence of hexa- and hepta-hydrated $MgSO_4$ species within the zeolite can provide a crucial function.

3.8 Dimer And Trimer Of hydrated magnesium sulfate in alpha FAU zeolite

The electronic energy of the hydrated dimer, $2(MgSO_4.2H_2O)$, is measured at -1279.748 eV, while the hydrated trimer, $3(MgSO_4.2H_2O)$, exhibits an electronic energy of -1347.199 eV.

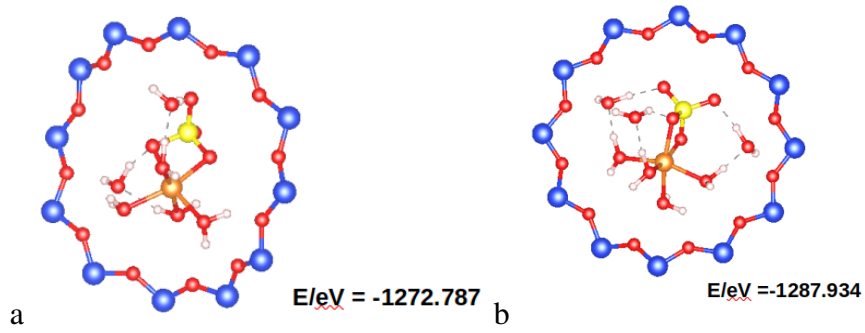

a b

Figure 29: a) Hexa-hydrated and b) Hepta-hydrated magnesium sulfate at super cages in FAU zeolite

Upon impregnation into alpha FAU zeolite, the adsorption energies for the dimer and trimer are found to be -5.069 eV and -42.082 eV, respectively. The notably higher adsorption energies of the hydrated trimer suggest a significantly stronger binding affinity between the trimer and the zeolite matrix compared to the dimer.

This translates to enhanced stability and immobilization of the hydrated trimer within the FAU-zeolite structure. In the context of thermal energy storage, the higher adsorption energy of the hydrated trimer implies a more efficient and reliable mechanism for capturing and storing thermal energy. The strong interaction between the trimer and the zeolite matrix allows for a greater capacity to absorb and retain heat, making it a promising candidate for thermal energy storage applications [42, 56]. The figure provided below illustrates a visual representation of the adsorption process, highlighting the robust interaction between the hydrated trimer and the FAU-zeolite.

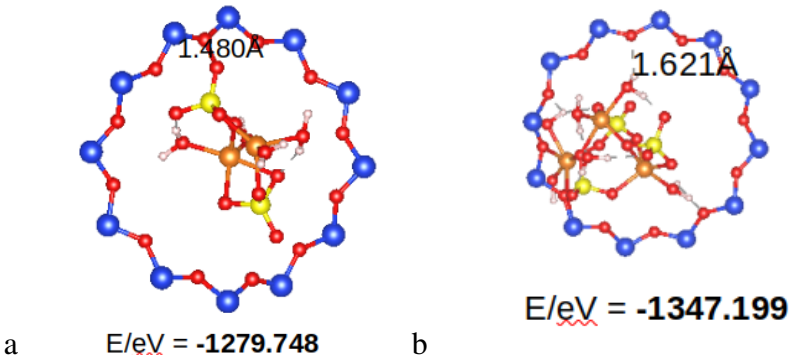

a b

Figure 30: Impregnated dimer and Trimer hydrated magnesium sulfate in alpha FAU zeolite

3.9 NaY-FAU zeolite framework and optimized composite structures of magnesium sulfate species

Zeolites are crystalline aluminosilicate minerals with a porous structure that enables them to function as catalysts and molecular sieves. Faujasite zeolite, or type X zeolite, is characterized by a three-dimensional pore structure made up of interconnecting cages and channels. Its large pore size and great heat stability make it a popular catalyst for isomerization and cracking reactions in the petroleum refining process [57].

Type Y Zeolite, often called ultrastable zeolite Y, is a modified form of Zeolite Type X. Its structure is more open, and its thermal stability is higher [37]. Due to their distinct qualities, Type X and Type Y zeolites are both appropriate for a variety of uses. The decision between the two is influenced by various elements, including the process's unique needs for catalysis or adsorption, temperature stability, and pore size requirements [2]. The figure below shows the structure of Y-FAU zeolite with a Si/Al ratio of 2.69 and Na at different sites for the charge balance when aluminum is introduced.

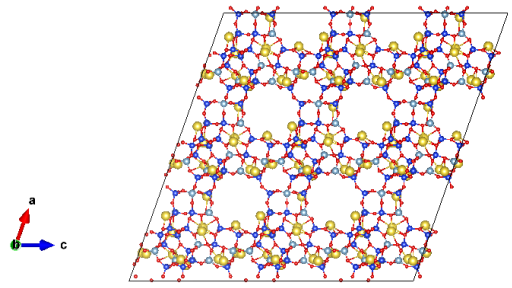

Figure 31: NaY-FAU zeolite structure

3.10 Impregnated $MgSO_4.H_2O$ and $MgSO_4.2H_2O$ to NaY-FAU

In figure 32, magnesium sulfate monohydrate ($MgSO_4 \cdot H_2O$) and a NaY-FAU (faujasite) zeolite with a silicon-to-aluminum (Si/Al) ratio of 2.69 make up the composite structure. The $MgSO_4 \cdot H_2O$ chemical can be incorporated into the porous framework structure of the NaY-FAU zeolite. This composite structure has an electronic energy of -1221.716 electron volts (eV), which suggests that its electronic arrangement is comparatively stable. The computed adsorption energy of -3.004 eV indicates a favorable and exothermic adsorption process, as it represents the energy released during the adsorption of $MgSO_4 \cdot H_2O$ into the NaY-FAU structure. Crucially, it is stated that the contact energy between the NaY-FAU

and $MgSO_4 \cdot H_2O$ components is positive, indicating the presence of an attractive interaction that aids in stabilizing the composite structure as a whole

Magnesium sulfate dihydrate ($MgSO_4 \cdot 2H_2O$) molecule can be incorporated into the porous framework structure of the NaY-FAU zeolite. This composite structure has a measured electronic energy of 1238.314 electron volts (eV), which suggests that its electronic arrangement has relatively high energy. It is computed that the adsorption energy is -3.521 eV and this also suggests that the adsorption process is favorable and exothermic.

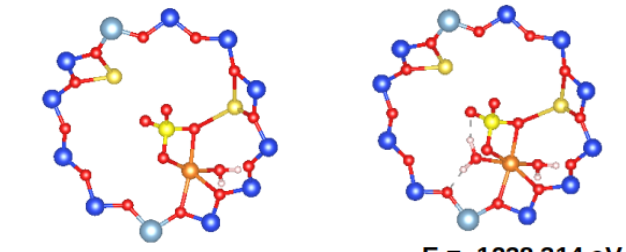

a b

Figure 32: Impregnated a) $MgSO_4.H_2O$ and b) $MgSO_4.2H_2O$to NaY-FAU in alpha opening

3.11 Impregnated $MgSO_4.3H_2O$ and $MgSO_4.4H_2O$ to NaY-FAU

The composite structures in figure 33 are made up of magnesium sulfate trihydrate ,$MgSO_4 \cdot 3H_2O$ or magnesium sulfate tetrahydrate ($MgSO_4 \cdot 4H_2O$) impregnated with NaY-FAU (faujasite) zeolite. The NaY-FAU zeolite has a framework structure that is porous enough to hold these magnesium sulfate hydrates. The composite structure with $MgSO_4 \cdot 3H_2O$ has an electronic energy of -1252.752 eV, whereas the composite structure with $MgSO_4 \cdot 4H_2O$ has an electronic energy of -1268.320 eV, suggesting rather stable electronic configurations.

For $MgSO_4 \cdot 3H_2O$ and $MgSO_4 \cdot 4H_2O$, the adsorption energies, which indicate the energy released during the adsorption of the magnesium sulfate hydrates into the NaY-FAU structure, are -2.74 eV and -3.155 eV, respectively. These values imply exothermic and advantageous adsorption processes.

It's significant to note that both magnesium sulfate hydrates and the NaY-FAU are reported to have positive interaction energies (2.740 & 3.155 eV), indicating the presence of an attractive interaction that aids in stabilizing the composite structures as a whole. It is notably underlined that the NaY-FAU zeolite framework's alpha apertures are where this positive interaction energy is impregnated.

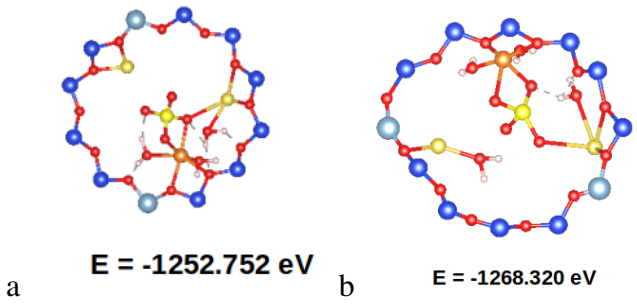

a b

Figure 33: Impregnated a) $MgSO_4.3H_2O$ and b) $MgSO_4.4H_2O$to NaY-FAU in alpha opening

3.12 Impregnated $MgSO_4.5H_2O$ and $MgSO_4.6H_2O$ to NaY-FAU

An electronic energy value of -1283.039 eV was measured for NaY-FAU with five water molecules and -1297.778 eV for the structure of NaY-FAU with six water molecules. Both -2.797 eV and -2.429 eV were the adsorption energies for penta and hexa hydrated magnesium sulfate. The adsorption characteristics and electronic structure of the composite materials are influenced by the hydration state, according to these findings.

The strength of the interaction between the adsorbent (the NaY-FAU framework) and the adsorbate (the $MgSO_4$ molecule in this instance) is indicated by the adsorption energy. In this case, the adsorption energy of the composite structure containing five water molecules is $MgSO_4.5H_2O$ is more negative at -2.797 eV than that of the structure including six water molecules, $MgSO_4.6H_2O$, at -2.429 eV. This implies that there is a stronger contact and increased adsorption between the $MgSO_4$ compound and the NaY-FAU framework as a result of the 5-water hydration state.

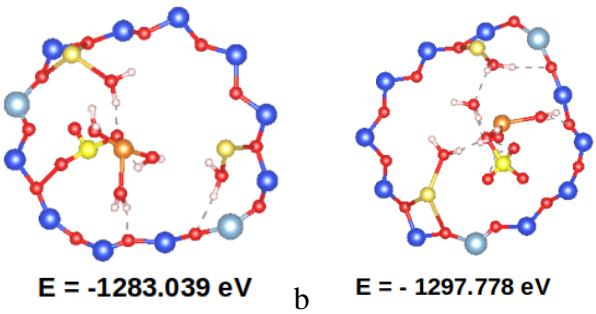

a b

Figure 34: Impregnated a)$MgSO_4.5H_2O$ and b)$MgSO_4.6H_2O$to NaY-FAU in alpha opening

3.13 Impregnated $MgSO_4.7H_2O$ to NaY-FAU

The composite structure of NaY-FAU and $MgSO_4$ with 7 water molecules was analyzed. The electronic energy of this structure was found to be -1301.804 eV. The adsorption

energy between the NaY-FAU framework and the $MgSO_4.7H_2O$ compound was -2.853 eV, indicating a strong interaction. The interaction energy of 2.853 eV further confirms the favorable binding between the components, suggesting this hydration state may be optimal for potential applications leveraging the adsorption properties of the composite material. Therefore, the adsorption process is more exothermic and spontaneous, the adsorbate is more firmly bonded to the adsorbent surface, and the adsorbate-adsorbent interaction is stronger. In summary, a comparison of the interaction energies between a conventional

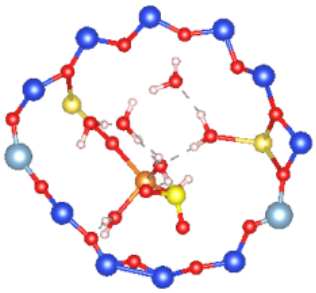

Figure 35: Impregnated $MgSO_4.7H_2O$ to NaY-FAU in alpha opening

FAU framework of silicon-oxygen (Si-O) and Y-type FAU zeolite with the charge balance cation of a sodium (NaY) framework with increasing amounts of water molecules is shown in figure 36 as a bar graph. The number of water molecules in hydrated magnesium sulfate varies from 0 to 7, and the interaction energy is expressed in electron volts (eV). The graph makes it clear that the interaction energy for the Si-O and NaY frameworks varies with the quantity of water molecules. This implies that the thermochemical characteristics of these frameworks may be strongly influenced by the hydration levels.

Higher interaction energies, for example, would suggest a stronger binding with water molecules, which might have an impact on the characteristics of thermal stability. The graph indicates that, for a given range of water molecule numbers per formula unit of magnesium sulfate, the interaction energies for the NaY zeolite (orange bars) are often higher than those for the Si-O zeolite (blue bars). In order to effectively store thermochemical energy and perform dehydration, it is imperative that the NaY zeolite framework be able to adsorb and desorb water molecules with greater strength and capacity.These interaction energies have important consequences for improved thermochemical characteristics in a composite composed of typical FAU frameworks of Si-O and NaY.The NaY zeolite, in particular, shows peak interaction energies of about 3.5 eV for two water molecules and about 3 eV

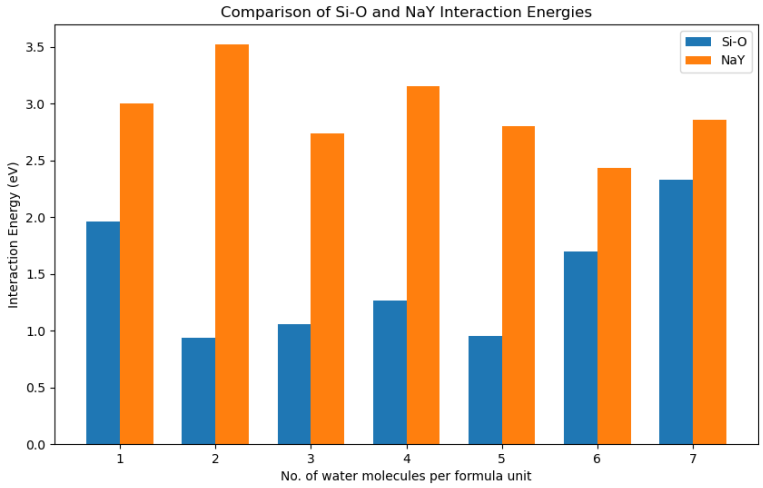

Figure 36: Interaction energy of composites made from normal Si-O and NaY FAU zeolites and hydrated magnesium sulfate.

for increasing numbers of water molecules.

The Si-O zeolite, on the other hand, exhibits interaction energies that are generally lower than 2.5 eV. The NaY zeolite framework's improved interaction energies suggest that it has the capacity to store and release energy during adsorption and desorption processes more effectively. The material's capacity to reversibly absorb and desorb water makes it an ideal feature for thermochemical energy storage system applications. Therefore, the NaY zeolite framework would be a better option than the Si-O zeolite to improve the thermochemical characteristics for energy storage and dehydration applications based on the interaction energy data that was supplied.

The deformation energy of a composite material impregnated into an FAU (faujasite) zeolite structure with hydrated magnesium sulfate ($MgSO_4 \cdot nH_2O$, where n = 1, 2,..., 7) is anticipated to exhibit a different pattern as the hydration level (n) of the $MgSO_4$ component varies. The FAU zeolite structure would be more stiff and might experience greater localized strain from the hydrated $MgSO_4$ species with lower water content (n = 1 or 2). In contrast to the more hydrated forms (n = 6 or 7), where the increased water content can better disperse and dissipate the deformation stresses throughout the composite, this could lead to a higher deformation energy need. A relatively small structural distortion is needed to integrate the mono-hydrated clusters into the FAU framework, according to the results, which demonstrate that the deformation energy for the composite structure of the FAU zeolite and mono-hydrated $MgSO_4$ is 0.047 eV. Based on this, it is possible that a stable

and well-integrated composite material will result from the high degree of compatibility and adaptability between the mono-hydrated $MgSO_4$ and the FAU zeolite structure.

Conversely, for composite structures containing more highly hydrated $MgSO_4$ clusters, the deformation energy increases dramatically. The deformation energy for the combination of FAU zeolite and tri-hydrated $MgSO_4$ is 0.254 eV, whereas the combination of FAU zeolite and tetra-hydrated $MgSO_4$ is 0.345 eV. The increased deformation energies suggest that the addition of the more hydrated$MgSO_4$ clusters to the FAU framework necessitates more structural reorganizations and significantly increases the strain in the composite. The design and optimization of the hydrated $MgSO_4$-FAU composite materials for thermochemical energy storage applications will be significantly impacted by these findings. Because the mono-hydrated composite has a low deformation energy and can be easily integrated into the FAU structure, it may be the most advantageous configuration in terms of stability and reversibility during the charging and discharging cycles.

On the other hand, the tri- and tetra-hydrated composites' greater deformation energies imply that these systems would not be as compatible with the FAU zeolite structure, which could result in increased structural strain and eventual degradation over time. By weighing the energy storage capacity against the material's structural integrity and long-term performance, this information can help determine the best hydration state for the $MgSO_4$ clusters to be added to the FAU composite.

4 Conclusion

An analysis of the molecular structures of $MgSO_4 \cdot nH_2O$, with n = 0, 1, 2, ... 7, was optimized using VASP software and conducted to understand the equilibrium curves for the dehydration reactions noted in these salt hydrates. DFT calculations have been performed to comprehend the equilibrium product concentrations of the dehydration a reaction of $MgSO_4.nH_2O$. The electrostatic force and strength of the created H-bond determines the relative stability of a conformer and the dehydration enthalpy. The dehydration curve of magnesium sulfate provides valuable information about the thermodynamic behavior, stability, and energy changes associated with the dehydration process. The energy changes that occur during dehydration can also be understood from the dehydration curve. The slope or steepness of the curve can represent the energy required or released during the removal of water molecules. Higher energy changes are indicated by steeper slopes, whereas lesser energy changes are indicated by flatter slopes.

Employing FAU-zeolites to make composite structures, which are crystalline aluminosilicate materials with well-defined porous structures characterized by their large cavities and interconnected channels, to study their adsorption properties. By using the Si/Al ratio of 2.69 as a balance between framework stability and adsorption. Sodium (Na) ions are used to balance the charge within the suggested zeolite framework, according to the proposed sites in the literature. These cations occupy specific sites and contribute to overall stability.In order to improve the thermochemical performance of sulfate-bearing hydrated materials, we looked into the stability, thermal energies, and structural characteristics of these materials using computational techniques.

The NaY zeolite framework would be a better option than the Si-O zeolite to improve the thermochemical characteristics for energy storage and dehydration applications based on the interaction energy data that was supplied. To achieve even greater thermochemical efficiency, future studies should concentrate on modifying the material's composition, crystal structure, and surface characteristics. Furthermore, practical applications will require an understanding of the dynamics of crystal formation and sulfate hydration. To sum up, the integration of customized zeolite materials with computational design principles has promising opportunities for enhancing thermochemical efficiency and tackling environmental issues. Scholars ought to persist in investigating these pathways in order to fully realize the possibilities of hydrated materials containing sulfate and FAU zeolites.

5 Limitation and Recommendation of the study

A multifaceted computational strategy is advised in order to improve comprehension and provide important data for the enhanced thermochemical performance of hydrated magnesium sulfate. To begin with, performing a simulated annealing process at various temperatures will offer insightful information about the system's energetics and structural stability, assisting in the determination of the best circumstances for energy storage. Furthermore, a more thorough investigation of the intricate energy landscape and the dynamic behavior of the composite materials will be made possible by the application of cutting-edge computational techniques like Monte Carlo simulations.

Furthermore, conducting composite structure analyses of $MgSO_4.nH_2O$'s with X- and Y-type zeolites in conjunction with matching frequency computations and Bader charge analysis will provide a more comprehensive comprehension of the charge distribution and intermolecular interactions inside the composites.The researchers can obtain a better understanding of the water-ion interactions, energy barriers, and charge transfer mechanisms by conducting Bader charge analysis and frequency calculations on these composite systems. This knowledge will eventually help design more effective and cyclable $MgSO_4$-based thermochemical energy storage materials.

By tackling the main obstacles and realizing the full potential of these materials for useful applications, the implementation of these suggested computational methodologies and analyses can greatly aid in the development of improved $MgSO_4$-based energy storage solutions. Clarifying the structural characteristics controlling the material's thermochemical behavior through these investigations is crucial for developing well-informed design principles and enhancing energy storage application performance.

References

[1] C. S. P. Aydin, Devrim and S. Riffat, "The latest advancements on thermochemical heat storage systems," *Renewable and Sustainable Energy Reviews*, vol. 41, pp. 356–367, 2015.

[2] Y. Hasegawa, T. Tanaka, K. Watanabe, B.-H. Jeong, K. Kusakabe, and S. Morooka, "Separation of $CO_2-CH_4$and CO_2-N_2 systems using ion-exchanged FAU-type zeolite membranes with different Si/Al ratios," *Korean Journal of Chemical Engineering*, vol. 19, pp. 309–313, 2002.

[3] A. U. Rehman, M. Z. Shah, S. Rasheed, W. Afzal, M. Arsalan, H. U. Rahman, M. Ullah, T. Zhao, I. Ullah, A. U. Din *et al.*, "Inorganic salt hydrates and zeolites composites studies for thermochemical heat storage," *Zeitschrift für Physikalische Chemie*, vol. 235, no. 11, pp. 1481–1497, 2021.

[4] R.-J. Clark, A. Mehrabadi, and M. Farid, "State of the art on salt hydrate thermochemical energy storage systems for use in building applications," *Journal of Energy Storage*, vol. 27, p. 101145, 2020.

[5] S. Gulati, Z. Tabassum, U. Schwingenschlogl, and E. Iype, "Molecular dynamics simulation of dehydration of salt hydrates ($MgSO_4 \cdot 7H_2O$ and $ZnSO_4 \cdot 7H_2O$)," *Materials Today: Proceedings*, vol. 28, pp. 1013–1017, 2020.

[6] A. Pathak, I. Tranca, S. Nedea, H. Zondag, C. Rindt, and D. Smeulders, "First-principles study of chemical mixtures of $CaCl_2$ and $MgCl_2$ hydrates for optimized seasonal heat storage," *The Journal of Physical Chemistry C*, vol. 121, no. 38, pp. 20 576–20 590, 2017.

[7] A. Pathak, S. Nedea, H. Zondag, C. Rindt, and D. Smeulders, "A DFT based equilibrium study of a chemical mixture tachyhydrite and their lower hydrates for long-term heat storage," in *Journal of Physics: Conference Series*, vol. 745, no. 3. IOP Publishing, 2016, p. 032003.

[8] S. Hongois, F. Kuznik, P. Stevens, and J.-J. Roux, "Development and characterization of a new $MgSO_4$-zeolite composite for long-term thermal energy storage," *Solar Energy Materials and Solar Cells*, vol. 95, no. 7, pp. 1831–1837, 2011.

[9] K. Linnow, M. Niermann, D. Bonatz, K. Posern, and M. Steiger, "Experimental studies of the mechanism and kinetics of hydration reactions," *Energy procedia*, vol. 48, pp. 394–404, 2014.

[10] S. Hongois, F. Kuznik, P. Stevens, and J.-J. Roux, "Development and characterization of a new $MgSO_4$-zeolite composite for long-term thermal energy storage," *Solar Energy Materials and Solar Cells*, vol. 95, no. 7, pp. 1831–1837, 2011.

[11] K. Posern and C. Kaps, "Calorimetric studies of thermochemical heat storage materials based on mixtures of $MgSO_4$ and $MgCl_2$," *Thermochimica Acta*, vol. 502, no. 1-2, pp. 73–76, 2010.

[12] A. D. Pathak, S. Nedea, H. Zondag, C. Rindt, and D. Smeulders, "A DFT-based comparative equilibrium study of thermal dehydration and hydrolysis of $CaCl_2$ hydrates and $MgCl_2$ hydrates for seasonal heat storage," *Physical Chemistry Chemical Physics*, vol. 18, no. 15, pp. 10 059–10 069, 2016.

[13] V. Van Essen, H. Zondag, J. C. Gores, L. Bleijendaal, M. Bakker, R. Schuitema, W. Van Helden, Z. He, and C. Rindt, "Characterization of $MgSO_4$ hydrate for thermochemical seasonal heat storage," 2009.

[14] E. Iype, S. V. Nedea, C. C. Rindt, A. A. van Steenhoven, H. A. Zondag, and A. Jansen, "DFT study on characterization of hydrogen bonds in the hydrates of $MgSO_4$," *The Journal of Physical Chemistry C*, vol. 116, no. 35, pp. 18 584–18 590, 2012.

[15] I.-M. Chou and R. R. Seal, "Magnesium and calcium sulfate stabilities and the water budget of mars," *Journal of Geophysical Research: Planets*, vol. 112, no. E11, 2007.

[16] B. Smeets, E. Iype, S. Nedea, H. Zondag, and C. Rindt, "A DFT based equilibrium study on the hydrolysis and the dehydration reactions of $MgCl_2$ hydrates," *The Journal of chemical physics*, vol. 139, no. 12, 2013.

[17] J. G. Vitillo, T. Fjermestad, M. D'Amore, M. Milanesio, L. Palin, G. Ricchiardi, and S. Bordiga, "On the structure of superbasic (MgO)n sites solvated in a faujasite zeolite," *Physical Chemistry Chemical Physics*, vol. 20, no. 27, pp. 18 503–18 514, 2018.

[18] J. Leszczynski, *Practical Aspects of Computational Chemistry-Methods, Concepts & Applications*. Springer, 2022.

[19] F. Jensen, *Introduction to computational chemistry*. John wiley & sons, 2017.

[20] F. E. M. J. J. Jacobs, PA and H. van Bekkum, *Introduction to zeolite science and practice*. Elsevier, 2001.

[21] A. Daouli, E. P. Hessou, H. Monnier, M.-A. Dziurla, A. Hasnaoui, G. Maurin, and M. Badawi, "Adsorption of NO, NO_2 and H_2O in divalent cation faujasite type zeolites: a density functional theory screening approach," *Physical Chemistry Chemical Physics*, vol. 24, no. 25, pp. 15 565–15 578, 2022.

[22] A. F. B. L. Morales-Pacheco, P and J. Domínguez, "Synthesis and structural properties of zeolitic nanocrystals ii: FAU-type zeolites," *The Journal of Physical Chemistry C*, vol. 113, no. 6, pp. 2247–2255, 2009.

[23] W. R. W. L. Xu, SZ and J. Zhu, "Performance characterizations and thermodynamic analysis of magnesium sulfate-impregnated zeolite 13x and activated alumina composite sorbents for thermal energy storage," *Energy*, vol. 167, pp. 889–901, 2019.

[24] W. Ji, H. Zhang, S. Liu, Z. Wang, and S. Deng, "An experimental study on the binary hydrated salt composite zeolite for improving thermochemical energy storage performance," *Renewable Energy*, vol. 194, pp. 1163–1173, 2022.

[25] H. Petitjean, C. Lepetit, Z. Nour, R. Poteau, I. del Rosal, and D. Berthomieu, "How CuI and NaI interact with faujasite zeolite? a theoretical investigation," *The Journal of Physical Chemistry C*, vol. 124, no. 51, pp. 28 026–28 037, 2020.

[26] M. Chebbi, S. Chibani, C. L. Paul, Jean-François, and M. Badawi, "Evaluation of volatile iodine trapping in presence of contaminants: A periodic dft study on cation exchanged-faujasite," *Microporous and Mesoporous Materials*, vol. 239, pp. 111–122, 2017.

[27] R. E. Fletcher, S. Ling, and B. Slater, "Violations of löwenstein's rule in zeolites," *Chemical Science*, vol. 8, no. 11, pp. 7483–7491, 2017.

[28] R. E. Fletcher, "The location and effect of aluminium in zeolites," Ph.D. dissertation, UCL (University College London), 2019.

[29] L. Martins, R. T. Boldo, and D. Cardoso, "Ion exchange and catalytic properties of methylammonium fau zeolite," *Microporous and mesoporous materials*, vol. 98, no. 1-3, pp. 166–173, 2007.

[30] J. Zhang and M. Dolg, "ABCluster: the artificial bee colony algorithm for cluster global optimization," *Physical Chemistry Chemical Physics*, vol. 17, no. 37, pp. 24 173–24 181, 2015.

[31] G. Sun, J. Kürti, P. Rajczy, M. Kertesz, J. Hafner, and G. Kresse, "Performance of the vienna ab initio simulation package (VASP) in chemical applications," *Journal of Molecular Structure: THEOCHEM*, vol. 624, no. 1-3, pp. 37–45, 2003.

[32] J. Hafner, "Ab-initio simulations of materials using vasp: Density-functional theory and beyond," *Journal of computational chemistry*, vol. 29, no. 13, pp. 2044–2078, 2008.

[33] T. G. W. Frisch, Michael J and J. R. Cheeseman, "Systematic model chemistries based on density functional theory: comparison with traditional models and with experiment," *Theoretical and Computational Chemistry*, pp. 679–707, 1996.

[34] J. Hafner, "Ab-initio simulations of materials using vasp: Density-functional theory and beyond," *Journal of computational chemistry*, vol. 29, no. 13, pp. 2044–2078, 2008.

[35] C. L. Tien and J. H. Lienhard, "Statistical thermodynamics/revised printing," *Washington*, 1979.

[36] D. A. McQuarrie, *statistical-mechanics*. New York Evanston san Francisco London, 1976.

[37] T. Ammouli, J.-L. Paillaud, H. Nouali, R. Stephan, M.-C. Hanf, P. Sonnet, and I. Deroche, "Insights into water adsorption in potassium-exchanged x-type faujasite zeolite: Molecular simulation and experiment," *The Journal of Physical Chemistry C*, vol. 125, no. 35, pp. 19 405–19 416, 2021.

[38] E. P. Hessou, L. A. Bédé, H. Jabraoui, A. Semmeq, M. Badawi, and V. Valtchev, "Adsorption of toluene and water over cationic-exchanged y zeolites: A DFT exploration," *Molecules*, vol. 26, no. 18, p. 5486, 2021.

[39] X. Tang, Z. Liu, L. Huang, W. Chen, C. Li, G. Wang, G. Li, X. Yi, and A. Zheng, "Violation or abidance of lowenstein's rule in zeolites under synthesis conditions?" *ACS Catalysis*, vol. 9, no. 12, pp. 10 618–10 625, 2019.

[40] C. Bläker, V. Mauer, C. Pasel, F. Dreisbach, and D. Bathen, "Adsorption mechanisms of ethane, ethene and ethyne on calcium-exchanged LTA and FAU-zeolites," *Adsorption*, pp. 1–18, 2023.

[41] A. Al Ezzi and H. Ma, "Equilibrium adsorption isotherm mechanism of water vapor on zeolites 3a, 4a, X, and Y," in *ASME International Mechanical Engineering Congress and Exposition*, vol. 58417. American Society of Mechanical Engineers, 2017, p. V006T08A059.

[42] A. Emelianova, C. Balzer, G. Reichenauer, and G. Y. Gor, "Adsorption-induced deformation of zeolites 4a and 13x: Experimental and molecular simulation study," *Langmuir*, vol. 39, no. 32, pp. 11 388–11 397, 2023.

[43] M. Fischer, "Density functional theory study of hydrophobic zeolites for the removal of triclosan from aqueous solution," *Environmental Science: Advances*, vol. 2, no. 8, pp. 1082–1098, 2023.

[44] P. Krokidas, E. D. Skouras, V. Nikolakis, and V. N. Burganos, "Simulated annealing effects on na-fau crystal reconstruction and sorption efficiency," *Molecular Simulation*, vol. 34, no. 10-15, pp. 1299–1309, 2008.

[45] G. Balasubramanian, S. Murad, R. Kappiyoor, and I. K. Puri, "Structure of aqueous $MgSO_4$ solution: dilute to concentrated," *Chemical Physics Letters*, vol. 508, no. 1-3, pp. 38–42, 2011.

[46] X. Zhang, Y. Zhang, and Q. Li, "Ab initio studies on the chain of contact ion pairs of magnesium sulfate in supersaturated state of aqueous solution," *Journal of Molecular Structure: THEOCHEM*, vol. 594, no. 1-2, pp. 19–30, 2002.

[47] Y. Marcus, "Ionic radii in aqueous solutions," *Chemical Reviews*, vol. 88, no. 8, pp. 1475–1498, 1988.

[48] M. Fernández, J. Klapp, L. D. G. Sigalotti, and F. Ruette, "Hydration study of $MgSO_4$ using different theoretical and model approaches.¿ is there a proton transfer?" *Chemical Physics Letters*, vol. 713, pp. 39–45, 2018.

[49] F. E. Genceli, M. Lutz, A. L. Spek, and G.-J. Witkamp, "Crystallization and characterization of a new magnesium sulfate hydrate $MgSO_4 \cdot 11H_2O$," *Crystal Growth and Design*, vol. 7, no. 12, pp. 2460–2466, 2007.

[50] K. Linnow, M. Niermann, D. Bonatz, K. Posern, and M. Steiger, "Experimental studies of the mechanism and kinetics of hydration reactions," *Energy procedia*, vol. 48, pp. 394–404, 2014.

[51] E. Iype, Z. S. A. Khalfay, R. G. Chaudhuri, and B. P. Kumar, "Epsomite dehydration: a molecular dynamics study," *Journal of Energy Storage*, vol. 20, pp. 337–343, 2018.

[52] D. B. Hassan, W. Rekik, H. Naïli, and T. Mhiri, "A new organically templated magnesium sulfate: structure, spectroscopic analysis, and thermal behaviour," *Chemical Papers*, vol. 68, pp. 210–216, 2014.

[53] C. Fang, X. Lu, W. Buijs, Z. Fan, F. E. G. Güner, M. A. van Huis, G.-J. Witkamp, and T. J. Vlugt, "Crystal structure, stability, and electronic properties of hydrated metal sulfates $MSO_4.(H_2O)n$ (M= Ni, Mg; n= 6, 7) and their mixed phases: A first principles study," *Chemical Engineering Science*, vol. 121, pp. 77–86, 2015.

[54] K.-D. Grevel, J. Majzlan, A. Benisek, E. Dachs, M. Steiger, A. D. Fortes, and B. Marler, "Experimentally determined standard thermodynamic properties of synthetic $MgSO_4 \cdot 4H_2O$ (starkeyite) and $MgSO_4 \cdot 3H_2O$: A revised internally consistent thermodynamic data set for magnesium sulfate hydrates," *Astrobiology*, vol. 12, no. 11, pp. 1042–1054, 2012.

[55] O. Rusal and O. Eremin, "Evaluation of the standard thermodynamic functions of hydrate sulfates of divalent metals (Ca,Mn,Cd,Fe,Zn,Cu,Mg,Ni,Co,andBe)," *Geochemistry International*, vol. 60, no. 10, pp. 981–994, 2022.

[56] V. Mauer, C. Bläker, C. Pasel, and D. Bathen, "Energetic characterization of faujasite zeolites using a sensor gas calorimeter," *Catalysts*, vol. 11, no. 1, p. 98, 2021.

[57] B. Liu, F. Chen, L. Zheng, J. Ge, H. Xi, and Y. Qian, "Synthesis and structural properties of hierarchically structured aluminosilicates with zeolite Y (FAU) frameworks," *RSC advances*, vol. 3, no. 35, pp. 15 075–15 084, 2013.

Appendices

Appendix A

1. Methodology details

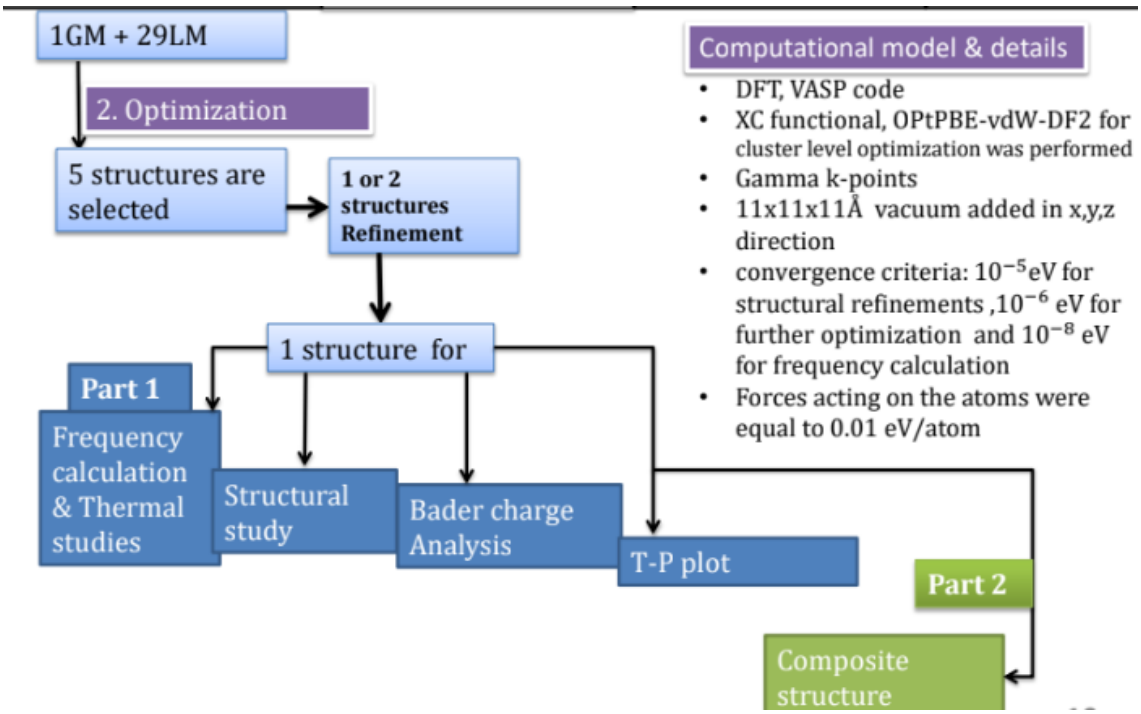

Figure 37: methodology details for structural refinements

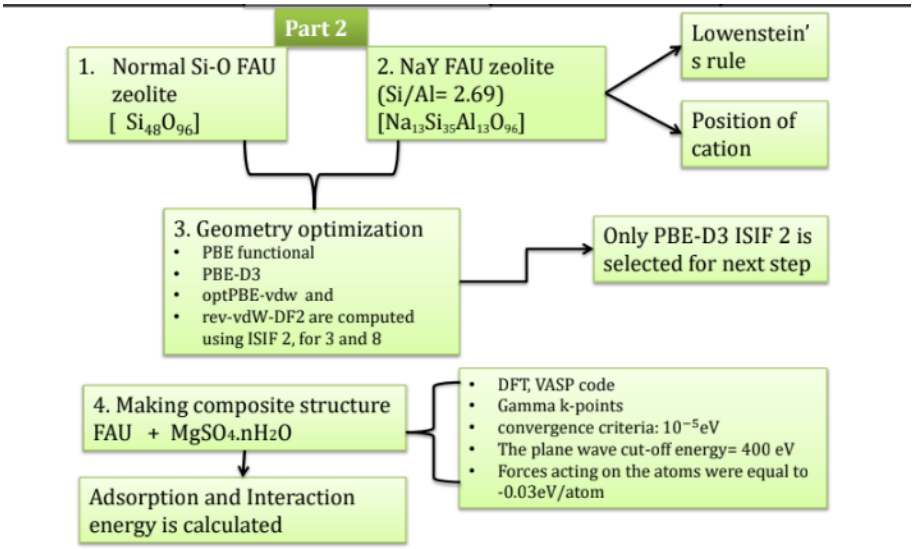

Figure 38: methodology details for composite structure optimization

2. Number of Hydrogen Bonds and Energies of Various Configurations 3. Intact water

Table 4: Number of Hydrogen Bonds and Energies of Various Configurations

molecule	Number of Hydrogen Bonds (HBn)	ΔE, *e*lectronic energy (eV)	References ([14])
$MgSO_4.1H_2O$	–	-35.512	-47.3
$MgSO_4.2H_2O$	1	- 48.567	-63.202
$MgSO_4.3H_2O$	1	-61.710	-78.870
$MgSO_4.4H_2O$	4	-74.791	-93.931
$MgSO_4.5H_2O$	4	-87.884	-109.111
$MgSO_4.6H_2O1$	6	-100.716	-123.500
$MgSO_4.6H_2O2$	5	-100.898	-124.168
$MgSO_4.7H_2O1$	7	-113.792	–
$MgSO_4.7H_2O2$	6	-113.804	–

for some structures that was experienced proton transfer

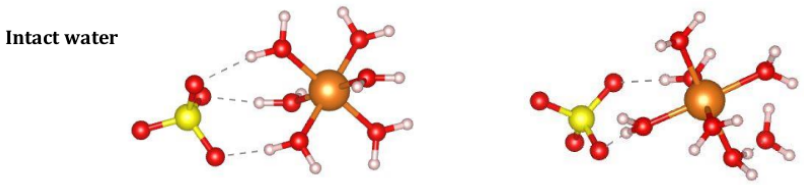

Figure 39: The intact water for hexa and hepta hydrated magnesium sulfate

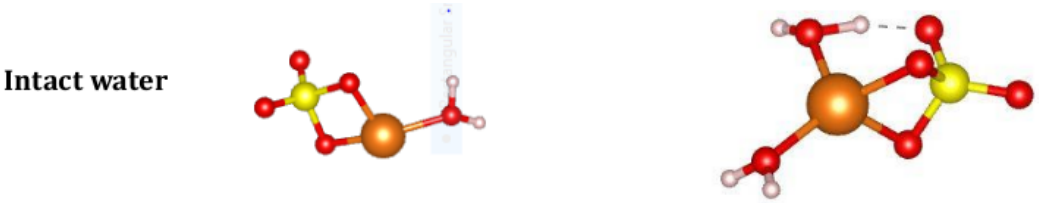

Figure 40: The intact water for mono and di hydrated magnesium sulfate

Appendix B

1. Relation between Gibbs free energy and enthalpy with T/K for the dehydration of $MgSO_4.nH_2O$

Figure 41: Relation between Gibbs free energy and enthalpy with T(K) for the dehydration of $MgSO_4.7H_2O$